

## Constructing resilient supply chain for risk-averse buyers by data-driven robust optimization approach

Yanjiao Wang <sup>a</sup>, Aixia Chen <sup>a</sup>, Naiqi Liu <sup>b</sup>, \*

<sup>a</sup> Hebei Key Laboratory of Machine Learning and Computational Intelligence, College of Mathematics & Information Science, Hebei University, Baoding 071002, Hebei, China

<sup>b</sup> College of Management and Economics, Tianjin University, Tianjin, 300072, China

### ARTICLE INFO

#### Keywords:

Resilient supply chain network  
Machine learning  
Data-driven robust optimization  
Supply chain risk management  
Benders decomposition

### ABSTRACT

Purchasing plays a crucial role in supply chain (SC) management, directly affecting the production and delivery of enterprises. The serious consequences caused by supply disruptions highlight the significance and necessity of preventing disruption. In addition, the economic panic and anxiety caused by disruptions have prompted SC managers to show a preference for risk avoidance. In this paper, based on diversified procurement and disruption prevention strategies, we study the problem of designing a resilient supply chain network (RSCN) that addresses supply disruption risks and uncertain demand for risk-averse buyers. The excess probability functional (EPF) indicator is innovatively customized to accommodate buyers' risk preferences. Regarding the uncertainty of demand, we utilize the support vector clustering (SVC) technique based on the given historical data to construct a data-driven uncertainty set and employ it to develop a data-driven robust optimization (DDRO) model. By linearization, epsilon-constraint method, and cone optimization theory, our proposed DDRO model can be reformulated as an equivalent tractable mixed integer linear programming (MILP) model and is solved by a new tailored Benders decomposition (BD) algorithm. Experiments under different settings are conducted on a real-world case, and the obtained results verify the validity of our proposed optimization method.

### 1. Introduction

Supply disruptions seriously impact the smooth flow and operation of products and services (Kumar et al., 2024). For instance, the 2011 Tohoku earthquake in Japan impacted multiple regional Toyota suppliers, leading to production halts and disruptions in their SC. The COVID-19 pandemic has caused a decline in supplier capacity and transportation disruptions in various areas, which has had an unprecedented and disruptive impact on global business and SC operations (Sarraf et al., 2024). In addition to macro-disruptions like natural disasters and pandemics, which have long-term impacts on SCs, there are also micro-disruptions such as human errors, extended lead times, and production failures that can affect daily SC operations in the short term (Chen et al., 2020). Although many companies and SCs have identified these issues, most buyers still face challenges in conducting risk assessments and implementing effective resilience strategies to recover from supply disruptions (Chowdhury et al., 2021; Lotfi et al., 2022a).

Establishing an effective SC resilience strategy is critical to mitigating and recovering from disruptions (Lotfi et al., 2023a). Hohenstein

et al. (2015) defined SC resilience as the preparedness of SCs to handle unexpected disruptions, along with their capability to rapidly respond and recover from these disruptions, ultimately returning to a standard or enhanced state. The traditional sourcing model of building a long-term partnership with a single major supplier can expose organizations to a significant supply disruption risk (Liu et al., 2024). Buyers frequently manage supply disruptions by employing strategies such as diversified sourcing, which involves procuring goods and services from multiple suppliers to reduce the risk of delivery failures (Wu et al., 2025). The existing literature emphasizes several advantages of diversified sourcing, including the reduction of supply risk through supplier diversification, the promotion of innovation and product improvement by fostering upstream competition, and the minimization of quality-related issues (Tang and Kouvelis, 2011; Li et al., 2017; Niu et al., 2019; Svoboda et al., 2021; Wu et al., 2025).

Developing and implementing an effective risk management method is an important means of mitigating the impact of supply disruptions and minimizing potential losses. For example, a recent survey

\* Corresponding authors.

E-mail addresses: [w\\_yanjiao@163.com](mailto:w_yanjiao@163.com) (Y. Wang), [chenaixia@hbu.edu.cn](mailto:chenaixia@hbu.edu.cn) (A. Chen), [nqliu@tju.edu.cn](mailto:nqliu@tju.edu.cn) (N. Liu).

<sup>1</sup> How COVID-19 is reshaping supply chains.

conducted by McKinsey & Company emphasized that in response to disruptions, companies are shifting towards risk-aversion strategic changes to their SCs.<sup>1</sup> Risk aversion is a common characteristic among individuals, indicating a preference for minimizing potential losses over seeking potential gains. This behavior is frequently observed in various decision-making contexts within operations management. Considering the decision-makers' attitude to risk, Lotfi et al. (2023b) adopted the entropic value at risk indicator for risk management. Sawik and Sawik (2024) applied stochastic optimization with Conditional Value at Risk (CVaR) to maintain risk-averse viability and enhance SC resilience under disruption propagation. Wang et al. (2024a) developed a distributionally robust optimization (RO) model for a resilient SC, incorporating the worst-case Mean-CVaR as a metric to capture the risk preferences of decision-makers.

Nowadays, SCs are vulnerable to uncertainty risks that can disrupt their operations, and thus, managers are looking for better ways to improve the robustness of resilient SCs (Pettit et al., 2019; Dixit et al., 2024; Wang et al., 2024b). To address this challenge, Artificial Intelligence has been used in risk management and in maintaining and improving SC resilience and robustness in this era of data explosion (Modgil et al., 2022; Fosso Wamba et al., 2024; Zackrisson et al., 2025). In this paper, we study the problem of RSCN design with diversified sources and preventing disruption strategies under the risk aversion criterion, providing possibilities for enhancing the resilience and robustness of SC. Through this study, the following research questions will be addressed:

**Q1.** How does adopting diversified procurement strategies and disruption prevention measures affect the cost-effectiveness and risk control of the SC in the event of supply disruptions and uncertain demand?

**Q2.** What are the advantages of our EPF risk measure for quantifying decision-makers' risk aversion compared to the commonly used CVaR risk measure?

**Q3.** What are the economic advantages of our RO method based on the machine learning technique in SC design decision-making?

Specifically, we first construct an uncertainty set to describe the uncertain demand parameters based on a large amount of data using a machine learning approach and then model a risk-averse resilient SC in the framework of RO. The developed DDRO model is equivalently transformed into a MILP model using duality techniques. Experimental results validate the effectiveness of our method. The main contributions of this paper are as follows:

- Risk management is incorporated into constructing a resilient SC, and diversified procurement and disruption prevention are utilized as resilience strategies. To our knowledge, our EPF indicator in this paper is used for the first time in RSCN design.
- Based on historical data, a new data-driven uncertainty set is constructed using the machine learning technique for uncertain demands, and the data-driven uncertainty set construction algorithm is implemented in the Python programming environment.
- A new DDRO model is developed to address the design problem of resilient SCs with uncertainty under the risk aversion criterion. The developed model is equivalently transformed into a MILP model, for which an effective BD algorithm is designed.
- The feasibility and effectiveness of the proposed optimization method and solution algorithm have been verified through a real case. The computational results demonstrate that the obtained robust decisions possess risk aversion ability and good resilience performance.

This paper is organized as follows. Section 2 presents a lucid exposition of the research value of this paper via the literature review. In Section 3, we furnish a detailed account of the problem and establish deterministic and DDRO models. Subsequently, we deduce an equivalent computationally tractable form of the proposed DDRO model in Section 4. In Section 5, we devise a BD algorithm to solve the proposed model. The efficacy and practical value of the model are validated through a real-world case study in Section 6. Finally, Section 7 summarizes this paper.

## 2. Literature review

This section reviews the literature regarding SC demand uncertainty, risk management and resilience strategies to identify meaningful research gaps.

### 2.1. SC demand uncertainty

Due to highly dynamic market fluctuations and unpredictable shifts in consumption patterns, a critical challenge in building RSCNs is effectively managing demand uncertainty (Chen and Chen, 2025). Various optimization approaches have been developed to address this challenge. Traditional approaches include stochastic programming, which models uncertain demand through probability distributions, as demonstrated by Lotfi et al. (2022a, 2023d) and Aghajani et al. (2023). Fuzzy programming represents another approach, where fuzzy set theory is applied to model uncertain demand in SC problems, as exemplified by Mohammed et al. (2023) through their application in the resilient multi-tier supplier selection and order allocation problem. RO has gained significant attention as an alternative framework for handling demand uncertainty without requiring precise probability distributions. Ben-Tal et al. (2009) developed RO frameworks that protect against worst-case scenarios within predefined uncertainty sets. Building on these foundations, Feng et al. (2022) extended RO approaches to multi-period SC problems with uncertain demands. More recently, scholars proposed distributionally RO approaches. These methods consider a family of probability distributions rather than a single distribution or uncertainty set. Feng et al. (2023) and Wang et al. (2024a) studied the design problem of multi-strategy RSCN with uncertain occurrence probability of each scenario through Box and Polyhedral ambiguity sets. In their works, demand uncertainty is indirectly reflected through different scenarios. Aiming at the RSCN design problem under the disruption scenario, Chen and Chen (2025) used the Wasserstein-moment ambiguity set to process the partial probability distribution information of the uncertain demand under consideration. Different from the above works, Goudarzi et al. (2023) incorporated different levels of demand variability into their study through game theory.

Despite these advances, there is still a significant research gap in utilizing historical data from the real world to construct uncertainty sets that reflect real demand patterns. Our work addresses this gap by developing a new method with SVC technique that can be applied to historical demand data. Unlike previous research, our method captures the actual patterns in real-world demand data, providing a more accurate and practical RO model for RSCN design problem.

### 2.2. SC risk management

SC risk management has been the subject of extensive research over the past decade. Regarding sources, SC risks include the supply, demand, and both sides. Considering the perspective of modeling approaches such as the risk preference of decision-makers and simulation methods have been adopted. A risk criterion and polyhedral DDRO method was proposed by Lotfi et al. (2024a) to model demand fluctuation. CVaR is a commonly used indicator in the literature to measure SC risk. For example, Gao et al. (2019) proposed a probabilistic method to assess disruption risks and measured SC resilience by analyzing the worst-case CVaR of total lost sales during disruptions, and Dixit et al. (2020) adopted CVaR as a risk measure to quantify worst-case resilience in high-severity risks. Aboytes-Ojeda et al. (2022) used CVaR and penalized value at risk to manage the risk of supply disruptions, and a two-stage stochastic model was developed to minimize the total cost and mitigate the impact of disruption risk. Lotfi et al. (2023d) quantified the inherent risks in SC management using the CVaR and developed a mathematical optimization model by integrating risk and robustness into the objective function via hybrid robust stochastic optimization technology. Feng et al. (2023) and Wang et al. (2024a)

incorporated the worst-case Mean-CVaR criterion into the cost analysis of the second stage, thereby balancing the expected cost with associated risks. In the field of viable vaccine SC network design, Lotfi et al. (2023c, 2024b) combined entropic value at risk with stochastic programming methods to handle risks. Unlike the above studies, Mhammadivojdan et al. (2022) utilized Karush–Kuhn–Tucker conditions along with Monte Carlo simulation to ascertain optimal procurement strategies amidst escalating uncertainties in the SC, and Zhang et al. (2024) strived for the sustainability of the service network by balancing goals under the uncertainty of demand.

However, most of the aforementioned studies have employed the CVaR indicator to measure the risk of SC disruptions, which reflects the average loss above a threshold value and is independent of the probability of exceeding the firm's budget. In this work, we introduce a probabilistic risk measure termed EPF to evaluate the risk level of the SC, marking its first application in RSCN research.

### 2.3. SC resilience strategies

Driven by increasing disruption risks and uncertainties, SC resilience has emerged as a critical research focus in recent years. Scholars have extensively investigated various resilience-enhancement strategies, particularly in supplier management and procurement approaches. Yin and Wang (2018) established a foundational framework for demand-determined SC strategies, emphasizing supplier diversification as a critical approach to risk mitigation. Fallahpour et al. (2021) contributed a fuzzy mathematical model designed to evaluate supplier efficiency through a resilience lens. Similarly, Lotfi et al. (2022b) introduced optimal vendor-managed inventory strategies to enhance resilience, while Suryadi and Rau (2023) implemented multi-faceted mitigation strategies, including geographically diverse suppliers and contingency shipping methods. Goudarzi et al. (2023) employed game theory to examine how SC managers choose between long-term and short-term contracts when balancing risk and individualism considerations. Building upon this foundation, a substantial body of literature has explored procurement strategies as resilience enhancement mechanisms. Within this stream, Azad and Hassini (2019) conducted comparative analyses of diversified sourcing versus sole sourcing in disruption-vulnerable networks. Han et al. (2023) proposed a dual-source procurement strategy to enhance the SC's stability. Aghajani et al. (2023) developed an integrated procurement-warehousing framework utilizing primary and contingency supplier contracts. Other contributions encompass Yoon et al. (2020)'s analysis of procurement decisions in three-tier SCs and the portfolio procurement model proposed by Wu et al. (2020), which integrates long-term contracts with spot market options. Disruption prevention has become a prominent proactive strategy in SC risk management. While Tang et al. (2014) established the foundational role of prevention strategies, Wu et al. (2025) advanced this field through integrated models that synergize preventive measures with contingency tactics. Their work demonstrated that strategic investments in prevention can significantly reduce vulnerability and enhance overall SC resilience.

The related literature mainly focuses on two supply strategies: integrating primary and backup suppliers or relying on the spot market. In addition, limited attention is paid to combining disruption prevention with advanced procurement methods. In contrast, taking into account the research gaps mentioned above, this work develops a comprehensive model that integrates diversified purchasing strategies, including three procurement channels: primary suppliers, backup suppliers, and spot markets. It also implements disruption prevention measures while using DDRO technology to manage the uncertain demands for risk-averse buyers.

### 2.4. Research gap

To better position this work, we summarize relevant literature in Table 1, which comprehensively analyzes 22 relevant papers covering various aspects of SC disruption, such as supply disruption handling, risk indicators, supply channel configuration, disruption prevention strategy, and optimization methods. Based on this extensive literature review, we identify the following research gaps.

- The current optimization methods in SC disruption literature rarely utilize historical data for uncertainty representation. Gao et al. (2019), Feng et al. (2022), and Liu et al. (2024) mainly rely on assumed probability distributions or simplified uncertainty sets, which may not fully capture the inherent complex patterns in real-world demand fluctuations. Although some researches, such as Lotfi et al. (2024a) and Chen and Chen (2025), have attempted to adopt distributionally RO methods, there is still a severe lack of methods that directly utilize real-world historical data to construct uncertainty sets that reflect actual demand patterns.
- Risk measurement in SC disruption literature is mainly centered around commonly used risk indicators such as CVaR (e.g., Dixit et al. (2020), Feng et al. (2023), Lotfi et al. (2023d) and Wang et al. (2024a)), which only capture the average loss exceeding a threshold value. Although some studies (e.g., Aboytes-Ojeda et al. (2022) and Lotfi et al. (2022a)) have attempted to employ alternative risk indicators such as penalized value at risk or entropic value at risk, these indicators still fail to reflect the probability of costs exceeding organizational budget thresholds directly.
- While SC resilience has been extensively studied, a notable gap exists in methods that simultaneously integrate all three supply channels (primary suppliers, backup suppliers, and spot market). Most existing studies, such as Aghajani et al. (2023) and Han et al. (2023), typically focus on only two supply channels. Moreover, only a few studies (e.g., Tang et al. (2014) and Wu et al. (2025)) address prevention mechanisms, and even fewer combine prevention with advanced risk management approaches.

Our research addresses these gaps by developing a comprehensive framework that (i) employs the SVC technique to construct a data-driven uncertainty set based on extensive historical demand data, thereby achieving both robustness and practical accuracy; (ii) introduces the EPF as a new risk indicator that can better capture the likelihood of costs exceeding critical thresholds and directly address organizational default risk; and (iii) incorporates all three procurement channels (primary suppliers, backup suppliers, and spot market) and integrates the disruption prevention strategy to enhance resilience. This holistic approach significantly demonstrates the value and innovation of our work.

## 3. Methodology

This section initially offers a detailed account of the studied RSCN design issue, followed by its modeling, where all parameters are supposed to be deterministic. Subsequently, we establish a data-driven uncertainty set based on SVC by employing a machine learning approach to depict the uncertainty of real-world demand and formulate a novel DDRO model for the RSCN design problem based on this uncertainty set.

### 3.1. Problem statement

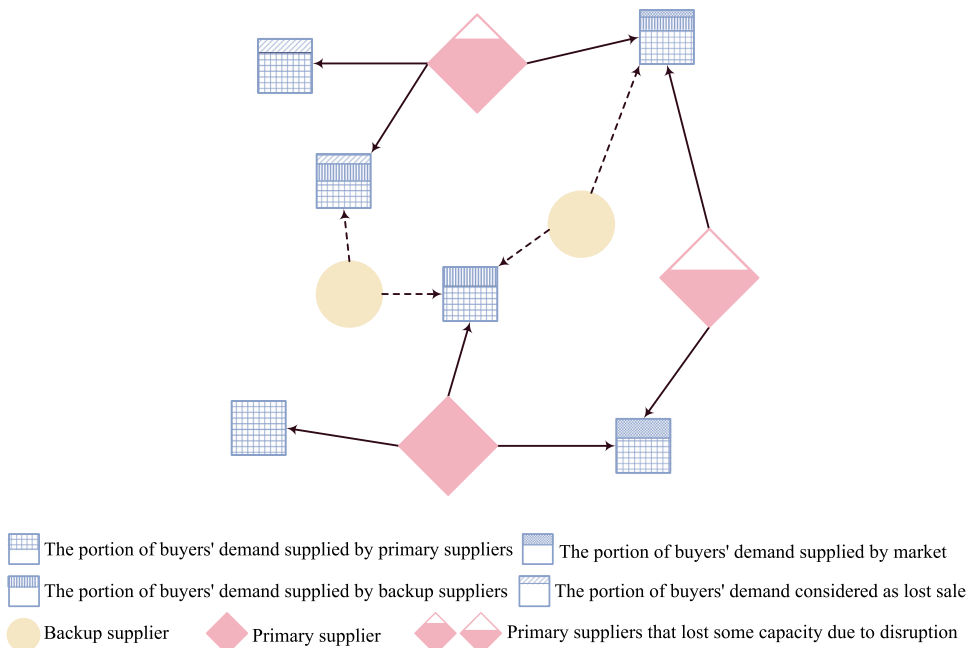
This paper focuses on the procurement of products by buyers from suppliers to meet their demands within an SC network system, where suppliers are susceptible to disruption risks, as shown in Fig. 1. Supply disruptions often lead to significant financial and operational losses.

**Table 1**

The position of this paper in the related literature.

Reference	Supply disruption	Risk indicator	Supply channel	Disruption prevention			Uncertainty	Optimization approach
				PS	BS	SM		
Tang et al. (2014)	✓	Null	✓	✓	✗	✓	Null	GT
Yin and Wang (2018)	✓	Null	✓	✓	✗	✗	Null	DO
Azad and Hassini (2019)	✓	Null	✓	✗	✓	✗	Recovery period	SP
Gao et al. (2019)	✓	VaR, CVaR	✓	✗	✗	✗	Null	DO
Dixit et al. (2020)	✓	CVaR	✓	✗	✗	✗	Null	DO
Wu et al. (2020)	✗	Null	✓	✗	✓	✗	Supply ratio	SP
Yoon et al. (2020)	✓	Null	✓	✗	✗	✗	Null	DO
Abeytes-Ojeda et al. (2022)	✗	CVaR	✓	✗	✗	✗	Supply raw material	SP
Feng et al. (2022)	✓	Null	✓	✓	✗	✗	Demand	RO
Lotfi et al. (2022a)	✓	EVaR	✓	✗	✗	✗	Demand	SP
Mohammadivjdan et al. (2022)	✓	Null	✓	✗	✓	✗	Interruption probability	SP
Aghajani et al. (2023)	✓	Null	✓	✓	✗	✗	Demand	SSP
Feng et al. (2023)	✓	CVaR	✓	✓	✗	✗	Interruption probability	DRO
Goudarzi et al. (2023)	✗	Null	✓	✗	✓	✗	Demand	GT
Han et al. (2023)	✓	Conservativeness	✓	✓	✗	✗	Interruption probability	GT
Lotfi et al. (2023d)	✓	CVaR	✓	✗	✗	✗	Demand	SP
Mohammed et al. (2023)	✗	Null	✓	✓	✗	✗	Demand	FP
Suryadi and Rau (2023)	✓	Risk scores	✓	✓	✗	✗	Null	DM
Liu et al. (2024)	✓	Null	✓	✓	✓	✗	Spot-market price	SP
Wang et al. (2024a)	✓	CVaR	✓	✗	✗	✗	Interruption probability	DRO
Wu et al. (2025)	✓	Null	✓	✓	✗	✓	Null	DO
Chen and Chen (2025)	✗	Null	✓	✓	✗	✗	Demand	DRO
This study	✓	EPF	✓	✓	✓	✓	Demand	SSP, DDRO

Note. PS: primary supplier; BS: backup supplier; SM: spot market; GT: game theory; DO: deterministic optimization; SP: stochastic programming; VaR: Value at Risk; CVaR: Conditional Value at Risk; EVaR: Entropic Value at Risk; SSP: scenario-based stochastic programming; DRO: distributionally robust optimization; FP: fuzzy programming; EPF: Excess Probability Functional; DDRO: data-driven robust optimization.

**Fig. 1.** The structure of the RSCN under disruption risk.

This study incorporates diversified sourcing and disruption prevention strategies in the design of an RSCN. Furthermore, the risk-averse behaviors of buyers are explicitly considered to better reflect real-world decision-making dynamics.

### 3.1.1. Diversified procurement

Diversified procurement refers to a buyer's strategy for sourcing products from multiple and distinct supply channels. One key advantage of this approach is its ability to help companies distribute risks more effectively and minimize exposure to potential disruptions. By adopting such a procurement model, buyers reduce their dependency

on any single supplier. In the event of a disruption affecting one supplier, alternative suppliers can step in to provide support, thereby serving as a hedge against supply disruption. Specifically, this paper considers the following supply sources:

**Multiple primary suppliers.** Due to geographical considerations, multiple potential primary suppliers are considered rather than merely one.

**Backup suppliers.** The buyer secures supply commitments from backup suppliers by paying an upfront retention fee, thereby ensuring their obligation to maintain a specified inventory level at a predetermined price.

**Spot purchasing.** The buyer has the flexibility to procure the required goods immediately at the prevailing market price.

The aforementioned diversified procurement strategy enables buyers to distribute their risks more effectively and reduce their vulnerability to supply disruption risks. In this context, buyers face complex procurement decisions involving multiple supply sources, making optimal allocation of procurement demands a critical operational challenge.

### 3.1.2. Disruption prevention

In addition to the diversified procurement strategy, investing in preventing disruption is another commonly used and effective method to reduce the risks of supply disruptions. Specifically, this study recommends that buyers invest in enhancing the early warning and recovery capabilities of their primary suppliers. Such investments enable suppliers to more effectively identify and address potential disruptions, thereby reducing risk exposure while ensuring the stability and continuity of the SC. Furthermore, these improvements contribute to smoother production and delivery processes, which in turn lower the supply risks faced by buyers. Ultimately, disruption prevention efforts are aimed at minimizing SC vulnerabilities, maintaining supply stability and continuity, and strengthening the resilience of the entire SC.

### 3.1.3. Risk aversion

The risk attitude of SC decision-makers reflects their perception, preferences, and capacity to manage risks, all of which significantly influence their decision-making processes in SC management. Risk aversion is a prevalent behavioral trait among individuals, characterized by a stronger inclination to avoid potential losses than to pursue equivalent gains. This behavioral tendency is commonly observed across various decision-making scenarios in SC operations management. Therefore, in the context of supply disruption risk, it is crucial to investigate how risk aversion impacts optimal decision-making and strategy formulation. For this purpose, we model the buyer as a risk-averse agent and introduce an EPF indicator to quantify the decision-maker's risk preference.

### 3.1.4. Assumptions

To formulate the RSCN design problem, we establish the following assumptions based on insights from existing literature and practical SC management experience:

**A1.** Primary suppliers may encounter disruptions, which lead to a partial loss of supply capacity. This assumption aligns with the widely documented reality of SC vulnerabilities found in risk management literature. Studies by Tang et al. (2014), Han et al. (2023) and Liu et al. (2024) demonstrated that supply disruptions typically lead to partial rather than total capacity losses. In our model, this phenomenon is captured through parameters that account for the occurrence and severity of disruptions, thereby enabling a more realistic depiction of SC risks.

**A2.** Backup suppliers are always regarded as available, and the simultaneous disruption of both primary and backup suppliers is considered negligible. Following the methodology proposed by Yin and Wang (2018), we assume that the backup supplier exhibits perfect reliability, thereby offering dependable emergency sourcing options. Although this assumption inevitably simplifies real-world complexities, it is widely adopted in the literature to isolate and examine the reliability challenges associated with primary suppliers while preserving the analytical tractability of the model.

**A3.** The buyer specifies a maximum allowable recovery time for the primary supplier following a disruption, commonly referred to as the extension of the maturity date. This time-based constraint integrates practical business considerations into our model framework. As suggested by Namdar et al. (2018), procurement decisions are driven by production schedules and customer delivery commitments, which effectively eliminate the possibility of indefinite supplier recovery periods in commercial procurement.

**Table 2**

The significance of each component of objective function (1a).

Component	Significance
$\sum_{m \in M} f_m X_m$	Contract costs with primary suppliers;
$\sum_{m \in M} \sum_{a \in A} s_{ma} Y_{ma}$	Procurement costs from primary suppliers;
$\sum_{b \in B} r_b Q_b$	Reserve costs for backup suppliers;
$\sum_{m \in M} \sum_{l \in L} g_{ml} Z_{ml}$	Setup cost of preventing disruption capability;
$\sum_{a \in A} \sum_{b \in B} o_{ba}^k V_{ba}^k$	Procurement costs from backup suppliers;
$\sum_{a \in A} q^k G_a^k$	Procurement costs from the market.

**A4.** The disruption prevention strategy is incorporated into the model by utilizing buyers' efforts to enhance suppliers' capabilities in terms of risk warning and recovery. This assumption is grounded in the buyer-supplier cooperation framework proposed by Tang et al. (2014), who demonstrated that buyers could provide incentives to improve supplier reliability. Our model operationalizes this concept by enabling buyers' efforts to enhance suppliers' warning and recovery levels.

These assumptions collectively shape our model in several important ways: they establish a realistic representation of supply disruptions, ensure the model's feasibility in extreme scenarios, incorporate actual time constraints that reflect business urgency, and achieve proactive risk management through collaborative investment. Together, these assumptions form a comprehensive framework that balances theoretical rigor with practical applicability in designing RSCN under uncertainty.

### 3.2. Development of deterministic model

Assuming all parameters are precisely known, we develop a deterministic benchmark model for the RSCN design problem. Relevant notations and their definitions used in constructing the mathematical model are summarized in Table A.1.

This paper adopts scenario-based modeling to capture the potential supply disruption risk through discrete scenarios. Each scenario includes disrupted and non-disrupted suppliers. Specifically, let  $M$  represent the set of primary suppliers and  $K$  denote the scenario set of primary supplier failures, then the scenario set can be represented as the combination of each primary supplier failure, i.e.,  $|K| = 2^{|M|}$ .

#### 3.2.1. Objective functions

Our primary objective is to minimize the expected total cost,

$$\min_{X, Y, Q, Z, V, G} \text{Obj}^1(X, Y, Q, Z, V, G),$$

where the primary objective is

$$\begin{aligned} \text{Obj}^1(X, Y, Q, Z, V, G) = & \sum_{m \in M} f_m X_m + \sum_{m \in M} \sum_{a \in A} s_{ma} Y_{ma} + \sum_{b \in B} r_b Q_b \\ & + \sum_{m \in M} \sum_{l \in L} g_{ml} Z_{ml} \\ & + \sum_{k \in K} p^k \sum_{a \in A} (\sum_{b \in B} o_{ba}^k V_{ba}^k + q^k G_a^k). \end{aligned} \quad (1a)$$

Moreover, the significance of each part is presented in Table 2.

In SC disruption, the consequences of exceeding budget thresholds are typically irreversible and severe, including reputation damage and production halts. This reality aligns with EPF's focus on threshold exceedance probability. Thus, we formulate the second objective using EPF indicator as follows,

$$\min_{X, Y, Q, Z, V, G} \text{Obj}^2(X, Y, Q, Z, V, G),$$

where the second objective function is

$$\text{Obj}^2(X, Y, Q, Z, V, G) = \Pr_p \{(\text{Cost}(X, Y, Q, Z; k) > C^0)\}, \quad (2a)$$

where  $\text{Cost}(X, Y, Q, Z; k) = \sum_{a \in A} (\sum_{b \in B} o_{ba}^k V_{ba}^k + q^k G_a^k)$  is the SC cost for each disruption scenario. This indicator quantifies the probability

that the cost surpasses the preselected threshold cost  $C^0$ , which is to be minimized. It reflects the risk-averse preference of decision-makers, who pay greater attention to maintaining cost control while avoiding potential risks (Schultz and Tiedemann, 2003).

### 3.2.2. Constraint conditions

The following constraints are established for the RSCN design problem,

$$\sum_{a \in A} Y_{ma} + \sum_{b \in B} V_{ba}^k + G_a^k \geq d_a^k \quad \forall k \in K, \forall a \in A, \quad (3a)$$

which guarantees that the total orders from primary suppliers, backup suppliers, and the market exceed the buyer's requirements.

$$\sum_{a \in A} Y_{ma} \leq (1 - i_m^k) c_m X_m + i_m^k c_m X_m \left[ n_m^k + \sum_{l \in L} T_m^k Z_{ml} v_{ml} \right] \quad \forall k \in K, \forall m \in M, \quad (3b)$$

which restrict the ordered quantity from the primary supplier to ensure compliance with its capacity limits. When the primary supplier is unaffected by disruptions ( $i_m^k = 0, \forall k \in K, \forall m \in M$ ), its full capacity is allocated to fulfilling demand. During disruption scenarios ( $i_m^k = 1, \forall k \in K, \forall m \in M$ ), the supplier meets the buyer's requirements using available and recovery capacity, where the latter is enabled by warning capacity that supports production resumption.

$$\sum_{a \in A} V_{ba}^k \leq Q_b \quad \forall k \in K, \forall b \in B, \quad (3c)$$

which ensure that the total procurement from backup suppliers does not exceed the reserved capacity.

$$T_m^k (1 - h_{ml} Z_{ml}) \leq t^{max} \quad \forall k \in K, \forall m \in M, \forall l \in L, \quad (3d)$$

these constraints stipulate that the cumulative time required for a supplier to restore a specific level of capability does not exceed the maximum allowable recovery time. This time limit is set by the buyer based on their tolerance for delays beyond due dates, and early warnings can accelerate the recovery process.

$$\sum_{l \in L} Z_{ml} = X_m \quad \forall m \in M, \quad (3e)$$

which mandate that if no contract exists with the supplier, the investment in disruption prevention for that supplier must be zero. Conversely, when supplier  $m$  is selected, specifying an effort level becomes mandatory. The corresponding variables are defined in constraints (3f) and (3g),

$$X_m, Z_{ml} \in \{0, 1\} \quad \forall m \in M, \forall l \in L, \quad (3f)$$

$$Y_{ma}, Q_b, G_a^k, V_{ba}^k, T_m^k \geq 0 \quad \forall m \in M, \forall a \in A, \forall b \in B, \forall k \in K. \quad (3g)$$

### 3.2.3. Deterministic model

Based on the previous work, the determined RSCN design model is formulated as follows,

$$\begin{cases} \min_{X, Y, Q, Z, V, G} \text{Obj}^1(X, Y, Q, Z, V, G) \\ \min_{X, Y, Q, Z, V, G} \text{Obj}^2(X, Y, Q, Z, V, G) \\ \text{s.t. Constraints (1a), (2a), (3a) - (3g).} \end{cases} \quad (4)$$

Deterministic RSCN model (4) is constructed on the premise that all parameters are precisely known, which is arduous to achieve in practical problems, such as demands filled with uncertainty. Therefore, we subsequently consider the RSCN design problem with uncertain demands.

### 3.3. Development of DDRO model

In this section, we use the historical demand data and SVC method to build a data-driven uncertainty set that meets certain confidence requirements and establish a DDRO model for the RSCN design problem based on this uncertainty set.

### 3.3.1. Building the uncertainty set

The SVC algorithm is based on support vector machines, mapping data points from a low-dimensional data space to a high-dimensional feature space through a kernel function. It then applies clustering algorithms to achieve data clustering. Specifically, within the feature space, SVC aims to identify the smallest hypersphere that contains the data image. This hypersphere is subsequently mapped back to the original data space, forming the boundary contour of the dataset, which is commonly referred to as the clustering boundary (Ben-Hur et al., 2001; Shang et al., 2017). In brief, SVC seeks to find the smallest volume closed ball that encompasses most or all data points in the dataset. The following section presents a data-driven method for constructing an uncertainty set grounded in SVC technique.

**Support vectors and uncertainty set.** Suppose  $\mathcal{D}^k = \{\mathbf{d}^k(j)\}_{j=1}^J$  ( $\mathbf{d}^k = \{d_1^k, d_2^k, \dots, d_{|A|}^k\}$ ) is a set of  $J$  requirement vector samples. Taking a fixed scenario as an example, the SVC algorithm for finding the minimum hypersphere can be translated into the following optimization problem,

$$\min_{R, C} \left\{ R^2 \mid \|\phi(\mathbf{d}(j) - C)\|^2 \leq R^2, \forall j \in \{1, \dots, J\} \right\}, \quad (5)$$

which means that after mapping the set  $\mathcal{D}$  to a high-dimensional feature space by a nonlinear mapping  $\phi(\cdot)$ , the radius  $R$  and center  $C$  of the minimum hypersphere are sought under the Euclidean distance  $\|\cdot\|$ . The constraint specified in model (5) is a “hard constraint”. To address potential outliers and prevent the occurrence of an excessive radius  $R$ , we introduce the relaxation variable  $\xi$  to convert this constraint into a “soft constraint”. This adjustment leads to the formulation of the following model,

$$\begin{aligned} & \min_{R, C, \xi} R^2 + \frac{1}{J\theta} \sum_{j \in \{1, \dots, J\}} \xi_j \\ & \text{s.t. } \|\phi(\mathbf{d}(j) - C)\|^2 \leq R^2 + \xi_j \quad \forall j \in \{1, \dots, J\}, \\ & \quad \xi_j \geq 0 \quad \forall j \in \{1, \dots, J\}, \end{aligned} \quad (6)$$

where  $\theta$  is the regularization parameter that implements the trade-off between the sphere's radius and the penalty term in the objective function of model (6). To solve model (6), we introduce Lagrange multipliers  $\alpha$  and  $\beta$  to define the Lagrange function as,

$$\begin{aligned} \mathcal{L}(R, C, \xi, \alpha, \beta) = & R^2 + \frac{1}{J\theta} \sum_{j \in \{1, \dots, J\}} \xi_j \\ & - \sum_{j \in \{1, \dots, J\}} \alpha_j (R^2 + \xi_j - \|\phi(\mathbf{d}(j) - C)\|^2) - \sum_{j \in \{1, \dots, J\}} \beta_j \xi_j. \end{aligned} \quad (7)$$

Following the first-order optimality condition, the function  $\mathcal{L}$  computes the first-order partial derivatives of  $R$ ,  $C$ , and  $\xi$ , and sets them to zero, then we obtain the following algebraic system,

$$\begin{cases} \sum_{j \in \{1, \dots, J\}} \alpha_j = 1, \\ C = \sum_{j \in \{1, \dots, J\}} \alpha_j \phi(\mathbf{d}(j)), \\ \alpha_j + \beta_j = \frac{1}{J\theta}. \end{cases} \quad (8)$$

After substituting Eq. (8) into Eq. (7), the dual of model (6) is as follows,

$$\begin{aligned} & \min_{\alpha} \sum_{j \in \{1, \dots, J\}} \sum_{i \in \{1, \dots, J\}} \alpha_i \alpha_j K(\mathbf{d}(j), \mathbf{d}(i)) - \sum_{j \in \{1, \dots, J\}} \alpha_j K(\mathbf{d}(j), \mathbf{d}(j)) \\ & \text{s.t. } 0 \leq \alpha_j \leq \frac{1}{J\theta} \quad \forall j \in \{1, \dots, J\}, \\ & \quad \sum_{j \in \{1, \dots, J\}} \alpha_j = 1, \end{aligned} \quad (9)$$

where  $K(\mathbf{d}(j), \mathbf{d}(i)) = \phi(\mathbf{d}(j))^T \phi(\mathbf{d}(i))$ . By combining the analysis and computation of Eqs. (8) and (9), we obtain the following conclusions. When  $\alpha_j > 0$ ,  $\|\phi(\mathbf{d}(j) - C)\|^2 \geq R^2$ , we know that  $\mathbf{d}(j)$  lies outside

the hypersphere and is classified as a support vector (SV). In contrast, when  $0 < \alpha_j < \frac{1}{J\theta}$ ,  $\|\phi(\mathbf{d}(j) - \mathbf{C})\|^2 = R^2$ ,  $\mathbf{d}(j)$  lies on the hypersphere, indicating a boundary support vector (BSV). Thus, the definitions of SV and BSV can be given as follows,

$$SV = \left\{ j \mid \alpha_j > 0, \forall j \in \{1, \dots, J\} \right\}, \quad (10)$$

$$BSV = \left\{ j \mid 0 < \alpha_j < \frac{1}{J\theta}, \forall j \in \{1, \dots, J\} \right\}. \quad (11)$$

Then the radius  $R$  can be determined as the distance between the center  $\mathbf{C}$  and any BSV  $\mathbf{d}(j')$ , i.e.,

$$\begin{aligned} R^2 &= \|\phi(\mathbf{d}(j') - \mathbf{C})\|^2 \\ &= K(\mathbf{d}(j'), \mathbf{d}(j')) - 2 \sum_{j \in \{1, \dots, J\}} \alpha_j K(\mathbf{d}(j'), \mathbf{d}(j)) \\ &+ \sum_{j \in \{1, \dots, J\}} \sum_{i \in \{1, \dots, J\}} \alpha_j \alpha_i K(\mathbf{d}(j), \mathbf{d}(i)) \quad j' \in BSV. \end{aligned} \quad (12)$$

Any data sample should be inside the hypersphere so that the data-driven uncertainty set can be expressed as,

$$\begin{aligned} \mathcal{U}(\mathcal{D}) = & \left\{ \mathbf{d} \mid K(\mathbf{d}, \mathbf{d}) - 2 \sum_{j \in \{1, \dots, J\}} \alpha_j K(\mathbf{d}, \mathbf{d}(j)) \right. \\ & \left. + \sum_{j \in \{1, \dots, J\}} \sum_{i \in \{1, \dots, J\}} \alpha_j \alpha_i K(\mathbf{d}(j), \mathbf{d}(i)) \leq R^2 \right\}. \end{aligned} \quad (13)$$

**Kernel function.** The weighted generalized intersection kernel function is defined as,

$$K(\mathbf{d}(j), \mathbf{d}(i)) = \sum_{j \in \{1, \dots, J\}} l_j - \|\bar{\mathbf{Q}}(\mathbf{d}(j) - \mathbf{d}(i))\|_1, \quad (14)$$

where  $\bar{\mathbf{Q}}$  is the weighted matrix and

$$l_j \geq \max_{i \in \{1, \dots, J\}} \bar{q}_j^T \mathbf{d}(i) - \min_{i \in \{1, \dots, J\}} \bar{q}_j^T \mathbf{d}(i), \quad (15)$$

with  $\bar{q}_j$  being the  $j$ th column of matrix  $\bar{\mathbf{Q}}$ . The expression of  $\bar{\mathbf{Q}}$  can be constructed based on the covariance matrix  $\Sigma$  of  $J$  samples, i.e.,

$$\begin{aligned} \bar{\mathbf{Q}} &= \Sigma^{-\frac{1}{2}}, \text{ and } \Sigma = \frac{1}{J-1} \left( \sum_{i \in \{1, \dots, J\}} \mathbf{d}(i)(\mathbf{d}(i))^T \right. \\ &\quad \left. - \left( \sum_{i \in \{1, \dots, J\}} \mathbf{d}(i) \right) \left( \sum_{i \in \{1, \dots, J\}} \mathbf{d}(i) \right)^T \right). \end{aligned} \quad (16)$$

In conclusion, our uncertainty set is constructed as follows:

$$\mathcal{U}(\mathcal{D}) = \left\{ \mathbf{d} \mid \sum_{j \in SV} \alpha_j \|\bar{\mathbf{Q}}(\mathbf{d} - \mathbf{d}(j))\|_1 \leq \tau \right\}, \quad (17)$$

where  $\tau = \min_{j' \in BSV} \sum_{j \in SV} \alpha_j \|\bar{\mathbf{Q}}(\mathbf{d}(j') - \mathbf{d}(j))\|_1$ . The pseudocode for the Python implementation of constructed data-driven uncertainty set (17) is summarized in Algorithm 1.

### 3.3.2. Formulating the DDRO model

Based on the SVC-based data-driven uncertainty set constructed in Section 3.3.1, we construct the following uncertainty set for  $\mathbf{d}^k$ ,

$$\mathcal{U}(\mathcal{D}^k) = \left\{ \mathbf{d}^k \mid \sum_{j \in SV^k} \alpha_j^k \|\bar{\mathbf{Q}}^k(\mathbf{d}^k - \mathbf{d}^k(j))\|_1 \leq \tau^k \right\}, \quad (18)$$

and establish the following DDRO model for our RSCN design problem,

$$\begin{cases} \min_{X, Y, Q, Z, V, G} \text{Obj}^1(X, Y, Q, Z, V, G) \\ \min_{X, Y, Q, Z, V, G} \text{Obj}^2(X, Y, Q, Z, V, G) \\ \text{s.t.} \quad \text{Constraints (1a), (2a), (3a) - (3g).} \end{cases} \quad (19)$$

It is noted that model (19) possesses a bi-objective structure, where the second objective takes the form of probability, and the constraints (3b) and (3d) are nonlinear. Moreover, since parameter  $\mathbf{d}^k$  can take any value within the uncertainty set  $\mathcal{U}(\mathcal{D}^k)$ , model (19) has semi-infinite constraints. Consequently, it cannot be solved directly. In the subsequent section, we will transform this model into its computationally tractable equivalent problem.

**Algorithm 1:** The pseudocode about building uncertainty set (17)

---

**Input:** Dataset  $\mathcal{D}$   
**Output:** Uncertainty set  $\mathcal{U}(\mathcal{D})$

- 1 \*\*\*\*\*Calculating the kernel function\*\*\*\*\*
- 2 Calculate the weighted matrix  $\bar{\mathbf{Q}}$  by substituting the dataset  $\mathcal{D}$  into Eq. (16);
- 3 Select the value of parameter  $l_j$  in accordance with Eq. (15) based on matrix  $\bar{\mathbf{Q}}$ ;
- 4 Substitute the weighted matrix  $\bar{\mathbf{Q}}$ , parameter  $l_j$ , and sample dataset  $\mathcal{D}$  into Eq. (14) and obtain the kernel matrix  $\mathbf{K} = \{K(\mathbf{d}(j), \mathbf{d}(i))\}$ .
- 5 \*\*\*\*\*Solving the support vector\*\*\*\*\*
- 6 Substitute the constructed kernel matrix  $\mathbf{K}$  into Eq. (9) and calculate  $\boldsymbol{\alpha}$  by minimizing it;
- 7 Establish the SV set and BSV set according to Eqs. (10) and (11), respectively.
- 8 \*\*\*\*\*Constructing the uncertainty set\*\*\*\*\*
- 9 Calculate the radius  $R$  in accordance with Eq. (12);
- 10 Substitute kernel matrix  $\mathbf{K}$  and radius  $R$  into Eq. (13) to obtain the explicit expression of the uncertainty set (17).
- 11 **return** Uncertainty set  $\mathcal{U}(\mathcal{D})$

---

## 4. Main results

This section is devoted to developing a computationally tractable system for model (19). We linearize constraints (3b) and (3d) in Section 4.1, handle the bi-objective in Section 4.2, and, in Section 4.3, we establish the robust counterpart for the DDRO model using cone optimization theory, guided by the properties of uncertainty set (18).

### 4.1. Linearizing constraints

The interaction between the variables  $T_m^k$  and  $Z_{ml}$  introduces nonlinearities into constraints (3b) and (3d), which we linearize separately.

**Constraints (3b).** Two non-negative continuous variables,  $\hat{\delta}_{ml}^k$  and  $\tilde{\delta}_{ml}^k$ , are introduced to linearize constraints (3b) as,

$$\hat{\delta}_{ml}^k + \tilde{\delta}_{ml}^k = v_{ml} T_m^k \quad \forall m \in M, \forall l \in L, \forall k \in K, \quad (20a)$$

$$\hat{\delta}_{ml}^k \leq N Z_{ml} \quad \forall m \in M, \forall l \in L, \forall k \in K, \quad (20b)$$

$$\hat{\delta}_{ml}^k \leq N(1 - Z_{ml}) \quad \forall m \in M, \forall l \in L, \forall k \in K, \quad (20c)$$

$$\hat{\delta}_{ml}^k, \tilde{\delta}_{ml}^k \geq 0 \quad \forall m \in M, \forall l \in L, \forall k \in K. \quad (20d)$$

Subsequently, constraints (3b) are presented as the following forms,

$$\sum_{a \in A} Y_{ma} \leq (1 - i_m^k) c_m X_m + i_m^k c_m X_m [n_m^k + \sum_{l \in L} \hat{\delta}_{ml}^k] \quad \forall k \in K, \forall m \in M. \quad (20e)$$

**Constraints (3d).** Two non-negative continuous variables,  $\hat{\gamma}_{ml}^k$  and  $\tilde{\gamma}_{ml}^k$ , are introduced to linearize constraints (3d) as,

$$\hat{\gamma}_{ml}^k + \tilde{\gamma}_{ml}^k = h_{ml} T_m^k \quad \forall m \in M, \forall l \in L, \forall k \in K, \quad (21a)$$

$$\hat{\gamma}_{ml}^k \leq N Z_{ml} \quad \forall m \in M, \forall l \in L, \forall k \in K, \quad (21b)$$

$$\hat{\gamma}_{ml}^k \leq N(1 - Z_{ml}) \quad \forall m \in M, \forall l \in L, \forall k \in K, \quad (21c)$$

$$\hat{\gamma}_{ml}^k, \tilde{\gamma}_{ml}^k \geq 0 \quad \forall m \in M, \forall l \in L, \forall k \in K. \quad (21d)$$

Subsequently, constraints (3d) are presented as,

$$T_m^k - \tilde{\gamma}_{ml}^k \leq t^{max} \quad \forall k \in K, \forall m \in M, \forall l \in L. \quad (21e)$$

As a result, nonlinear constraints (3b) and (3d) can be replaced by the equivalent algebraic systems (20) and (21), respectively.

#### 4.2. Handling objective functions

**Reformulate the second objective function.** Given that the feasible region of the decision variables  $(X, Y, Q, Z)$  is bounded in model (19), the second risk objective (2a) can be reformulated as follows,

$$\min_{X, Y, Q, Z, V, G, \rho} \text{Obj}^{2'}(X, Y, Q, Z, V, G, \rho) \quad (22a)$$

$$\text{s.t. } \text{Obj}^{2'}(X, Y, Q, Z, V, G, \rho) = \sum_{k \in K} p_k \rho_k, \quad (22b)$$

$$\text{Cost}(X, Y, Q, Z; k) - (N - C^0) \rho_k \leq C^0 \quad \forall k \in K, \quad (22c)$$

where  $\rho_k$  is a binary variable that serves as a statistical parameter to count the frequency of validity of the constraint  $\text{Cost}(X, Y, Q, Z; k) \leq C^0$ . Constraints (22c) are valid when the cost exceeds  $C^0$  and conversely, the opposite outcome prevails.

**Deal with bi-objective using the epsilon-constraint method.** The epsilon-constraint method is a multi-objective optimization algorithm founded on the notion of constrained optimization. It introduces a parameter  $\epsilon$  to regulate the weight of the objective function, thereby obtaining an approximate solution set that complies with the constraints while guaranteeing the attainment of the optimal solution. Specifically, we choose objective (1) as the principal objective and employ the epsilon-constraint method to transform problem (19) into the following problem,

$$\begin{cases} \min_{X, Y, Q, Z, V, G} \text{Obj}^1(X, Y, Q, Z, V, G) \\ \text{s.t. } \text{Obj}^{2'}(X, Y, Q, Z, V, G, \rho) \leq \epsilon, \quad \forall d^k \in \mathcal{U}(\mathcal{D}^k), \\ \text{Constraints (1a), (3a), (3c), (3e)} \\ \quad - (3g), (20), (21), (22b), (22c), \end{cases} \quad (23)$$

where the parameter  $\epsilon$  is computed based on Algorithm 2.

---

#### Algorithm 2: The pseudocode about computing parameter $\epsilon$

```

Input: Model (19)
Output: Parameter  $\epsilon$ 
1 for  $j \in \{1, 2'\}$  do
2   Solve the optimal solution  $(X_*^j, Y_*^j, Q_*^j, Z_*^j, V_*^j, G_*^j)$  of the
     objective  $\text{Obj}^j$ ;
3   Substitute  $(X_*^j, Y_*^j, Q_*^j, Z_*^j, V_*^j, G_*^j)$  into objective  $\text{Obj}^{2'}$ .
4 Determine the optimal and pessimal values for  $\text{Obj}^{2'}$ :
   $\text{Obj}_{\text{optimal}}^{2'} = \text{Obj}^{2'}(X_*^{2'}, Y_*^{2'}, Q_*^{2'}, Z_*^{2'}, V_*^{2'}, G_*^{2'})$ ;
   $\text{Obj}_{\text{pessimal}}^{2'} = \text{Obj}^{2'}(X_*^1, Y_*^1, Q_*^1, Z_*^1, V_*^1, G_*^1)$ .
5 Obtain  $\epsilon \in [\text{Obj}_{\text{optimal}}^{2'}, \text{Obj}_{\text{pessimal}}^{2'}]$ .

```

---

#### 4.3. Dealing with robust counterpart

Based on the worst-case criterion, our proposed DDRO model (19) can be reformulated as the following equivalent model,

$$\min_{X, Y, Q, Z, V, G} \text{Obj}^1(X, Y, Q, Z, V, G) \quad (24a)$$

$$\text{s.t. } \text{Obj}^{2'}(X, Y, Q, Z, V, G, \rho) \leq \epsilon, \quad (24b)$$

$$\sum_{m \in M} Y_{ma} + \sum_{b \in B} V_{ba}^k + G_a^k \geq \max_{d^k \in \mathcal{U}(\mathcal{D}^k)} d_a^k \quad \forall k \in K, \forall a \in A, \quad (24c)$$

$$\text{Constraints (1a), (3c), (3e)} - (3g), (20), (21), (22b), (22c). \quad (24d)$$

To deal with constraints (24c), we transform uncertainty set (18) as follows,

$$\mathcal{U}(\mathcal{D}^k) := \left\{ \mathbf{d}^k \left| \begin{array}{l} \exists \Psi_j^k, \quad \forall j \in SV^k \\ \text{s.t. } \sum_{j \in SV^k} \alpha_j^k (\Psi_j^k)^T \mathbf{1} \leq \tau^k, \\ - \Psi_j^k \leq \bar{Q}^k (\mathbf{d}^k - \mathbf{d}^k(j)) \leq \Psi_j^k \quad \forall j \in SV^k. \end{array} \right. \right\}. \quad (25)$$

In light of the structure of uncertainty set (25), the equivalent transformation about constraints (24c) is summarized in the following theorem.

**Theorem 1.** When  $0 < \theta < 1$ , semi-infinite constraint (24c) is equivalent to the following algebraic system:

$$\sum_{m \in M} Y_{ma} + \sum_{b \in B} V_{ba}^k + G_a^k \geq \sum_{j \in SV^k} (\Gamma_j^{ak} - Y_j^{ak})^T \times \bar{Q}^k d^k(j) + \Omega^{ak} \tau^k \quad \forall k \in K, \forall a \in A, \quad (26a)$$

$$\sum_{j \in SV^k} \bar{\Omega}^k (\Gamma_j^{ak} - Y_j^{ak}) + e^{ak} = \mathbf{0} \quad \forall k \in K, \forall a \in A, \quad (26b)$$

$$\Gamma_j^{ak} + \Gamma_j^{ak} = \Omega^{ak} \alpha_j^k \mathbf{1} \quad \forall j \in SV^k, \forall k \in K, \forall a \in A, \quad (26c)$$

$$\Gamma_j^{ak}, \Gamma_j^{ak} \in R_+^{|\Lambda|}, \Omega^{ak} \in R_+, \forall j \in SV^k, \forall k \in K, \forall a \in A. \quad (26d)$$

**Proof.** The proof of theorem is shown in Appendix B.  $\square$

To conclude, our DDRO model is equivalently transformed into the following MILP model,

$$\min_{X, Y, Q, Z, V, G, \delta, \hat{\delta}, \hat{y}, Y, \Gamma, Q} \text{Obj}^1(X, Y, Q, Z, V, G) \quad (27a)$$

$$\text{s.t. } \text{Obj}^{2'}(X, Y, Q, Z, V, G, \rho) \leq \epsilon, \quad (27b)$$

$$\text{Constraints (1a), (3c), (3e)} - (3g), \\ (20), (21), (22b), (22c), (26). \quad (27c)$$

So far, our DDRO model (19) has been converted into MILP model (27). In next section, we design a BD algorithm for the DDRO model following the structural characteristics of its equivalent algebraic system (27).

#### 5. Solution approach

The BD algorithm, which decomposes the problem into a relaxed Benders master problem (BMP) and Benders subproblem (BSP) and iteratively incorporates feasibility and optimality cuts to approximate the optimal solution, is an effective method for solving mixed-integer linear algebraic systems. In this paper, we partition the problem into the BMP and BSP based on the variable types: boolean variables and continuous variables. More precisely, after solving the BMP to determine the values of the computationally challenging boolean variables, the remaining problem is reduced to a standard linear programming problem. Subsequently, the cutting plane method is applied to appropriately represent the extremum of the BMP (with the solutions of the BSP as parameters) and the set of parameter values that render the BSP feasible. Duality theory is employed throughout this process to derive the natural cutting plane family characterizing these expressions. The following subsection provides a detailed description of each component of our BD algorithm.

Based on the structural characteristics of MILP model (27), the BMP, BSP, Benders feasibility cut, and Benders optimality cut are constructed as follows. Firstly, the BSP for model (27) is built as,

$$\begin{aligned} \min_{Y, Q, V, G, \delta, \hat{\delta}, \hat{y}, Y, \Gamma, Q} & \sum_{m \in M} \sum_{a \in A} s_{ma} Y_{ma} + \sum_{b \in B} r_b Q_b \\ & + \sum_{k \in K} p^k \sum_{a \in A} \left( \sum_{b \in B} \alpha_{ba}^k V_{ba}^k + q^k G_a^k \right) \end{aligned} \quad (28a)$$

$$\text{s.t. } \tilde{\delta}_{ml}^k \leq N Z_{ml}^* \quad \forall m \in M, \forall l \in L, \forall k \in K, \quad (28b)$$

$$\hat{\delta}_{ml}^k \leq N(1 - Z_{ml}^*) \quad \forall m \in M, \forall l \in L, \forall k \in K, \quad (28c)$$

$$\sum_{a \in A} Y_{ma} \leq (1 - i_m^k)c_m X_m^* + i_m^k c_m X_m^* n_m^k \\ + \sum_{l \in L} \hat{\delta}_{ml}^k \quad \forall k \in K, \forall m \in M, \quad (28d)$$

$$\hat{\gamma}_{ml}^k \leq N Z_{ml}^* \quad \forall m \in M, \forall l \in L, \forall k \in K, \quad (28e)$$

$$\hat{\gamma}_{ml}^k \leq N(1 - Z_{ml}^*) \quad \forall m \in M, \forall l \in L, \forall k \in K, \quad (28f)$$

$$\sum_{a \in A} \left( \sum_{b \in B} o_{ba}^k V_{ba}^k + q^k G_a^k \right) - (N - C^0)o_k^* \leq C^0 \quad \forall k \in K, \quad (28g)$$

Constraints (3c), (3g), (20a), (20d),

$$(21a), (21d), (21e), (26), \quad (28h)$$

where  $X_m^*$ ,  $Z_{ml}^*$ ,  $\rho_k^*$  are the optimal solution of the following BMP model.

$$\min_{X, Z, \rho} \sum_{m \in M} f_m X_m + \sum_{m \in M} \sum_{l \in L} g_{ml} Z_{ml} + U \quad (29a)$$

$$\text{s.t. } \sum_{k \in K} p_k \rho_k \leq \varepsilon, \quad (29b)$$

$$\text{Constraints (3e), (3f),} \quad (29c)$$

where  $U$  is a continuous auxiliary variable that assists in establishing the coupling relationship between the BMP and the BSP. This coupling relationship is formally characterized by the subsequent **Benders feasibility cuts** and **Benders optimality cuts**.

We introduce  $\bar{w}^i (i = 1, 2, \dots, 17)$  as dual variables for constraints (28b)–(28g), (3c), (3g), (20a), (20d), (21a), (21d), (21e), (26a)–(26d), respectively. The Benders feasibility cut is constructed as the following form,

$$0 \geq - \sum_{k \in K, m \in M, l \in L} N Z_{ml} \bar{w}_{kml}^1 - \sum_{k \in K, m \in M, l \in L} N(1 - Z_{ml}) \bar{w}_{kml}^2 \\ - \sum_{k \in K, m \in M} ((1 - i_m^k)c_m X_m + i_m^k c_m (n_m^k X_m)) \bar{w}_{km}^3 \\ - \sum_{k \in K, m \in M, l \in L} N Z_{ml} \bar{w}_{kml}^4 - \sum_{k \in K, m \in M, l \in L} N(1 - Z_{ml}) \bar{w}_{kml}^5 \\ + \sum_{k \in K} (-C^0 - (N - C^0)\rho_k) \bar{w}_k^6 - \sum_{k \in K, m \in M} t^{max} * \bar{w}_{km}^{13} - \sum_{a \in A, k \in K} e^{ak} \bar{w}_{ak}^{15}, \quad (30)$$

where  $\{\bar{w}^i | i = 1, 2, \dots, 17\}$  represent the extreme rays within the feasible region of BSP duality. Furthermore, the Benders optimality cut is constructed as the following form,

$$U \geq - \sum_{k \in K, m \in M, l \in L} N Z_{ml} \bar{w}_{kml}^1 - \sum_{k \in K, m \in M, l \in L} N(1 - Z_{ml}) \bar{w}_{kml}^2 \\ - \sum_{k \in K, m \in M} ((1 - i_m^k)c_m X_m + i_m^k c_m (n_m^k X_m)) \bar{w}_{km}^3 \\ - \sum_{k \in K, m \in M, l \in L} N Z_{ml} \bar{w}_{kml}^4 - \sum_{k \in K, m \in M, l \in L} N(1 - Z_{ml}) \bar{w}_{kml}^5 \\ + \sum_{k \in K} (-C^0 - (N - C^0)\rho_k) \bar{w}_k^6 - \sum_{k \in K, m \in M} t^{max} * \bar{w}_{km}^{13} - \sum_{a \in A, k \in K} e^{ak} \bar{w}_{ak}^{15}, \quad (31)$$

where  $\{\bar{w}^i | i = 1, 2, \dots, 17\}$  represent the extreme points within the feasible region of BSP duality problem.

Based on the definitions of the aforementioned BMP, BSP, Benders feasibility and optimality cuts, the process to solve problem (27) is presented as Algorithm 3.

## 6. Numerical experiments on a real case

In this section, we use the RSCN design issue of the electrolyte in the FinDreams Battery as a case study and conduct a series of

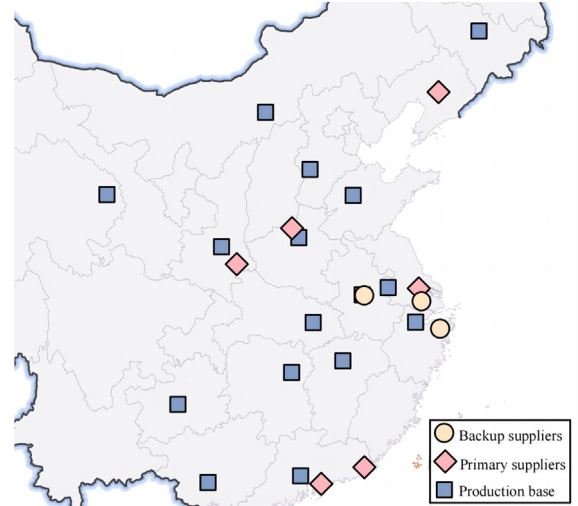


Fig. 2. Location of RSCN members.

**Algorithm 3:** The pseudocode about BD algorithm for solving problem (27)

```

Input:  $UB = \infty$ ,  $LB = -\infty$ ,  $Ta$  (Tolerability) =  $10^{-6}$ 
Output: The optimal solution of DDRO model (27)
1 while  $UB - LB \geq Ta$  do
2   Solve the BMP to obtain solution  $(X^*, Z^*, \rho^*, U^*)$ , and
      optimal objective value  $Obj_{BMP}^*$ ;
3   Update  $LB = \max\{LB, Obj_{BMP}^*\}$ ;
4   Solve the BSP using  $(X^*, Z^*, \rho^*)$ ;
5   if  $BSP$  is infeasible then
6     Obtain the extreme rays and construct Benders
      feasibility cuts via (30);
7     Incorporate these feasibility cuts into the BMP;
8   else
9     Obtain the extreme points and optimal objective value
       $Obj_{BSP}^*$ , construct Benders optimality cuts via (31);
10    Incorporate these optimality cuts into the BMP;
11    Update  $UB = \min\{UB, Obj_{BMP}^* - U^* + Obj_{BSP}^*\}$ .
12 Obtain optimal solution.

```

experiments to evaluate the effectiveness of the proposed model. Section 6.1 provides a detailed background. In Section 6.2, we demonstrate the superiority of the proposed DDRO model by comparing it with the deterministic and budgeted robust optimization (BRO) models. Section 6.3 investigates the benefits of diversified procurement. In Section 6.4, we analyze the impact of risk preferences. Our EPF indicator is compared with the commonly used CVaR indicator in Section 6.5. A series of sensitivity analyses are carried out in Section 6.6. Finally, Section 6.7 summarizes the key management insights. All experiments are conducted on a Windows 11 computer with 32 GB of memory and an Intel Core i5 processor.

### 6.1. Description of the case and data source

In the ecosystem of new energy vehicles, traction batteries serve as the core component that drives the operation of electric vehicles. FinDreams Battery is a renowned battery manufacturer, and its batteries are installed in the currently popular Xiaomi SU7. In this study, we apply the proposed DDRO model to the RSCN design issue of this manufacturer's electrolyte. The electrolyte is a key material indispensable for battery production, and the resilience of its SC is important

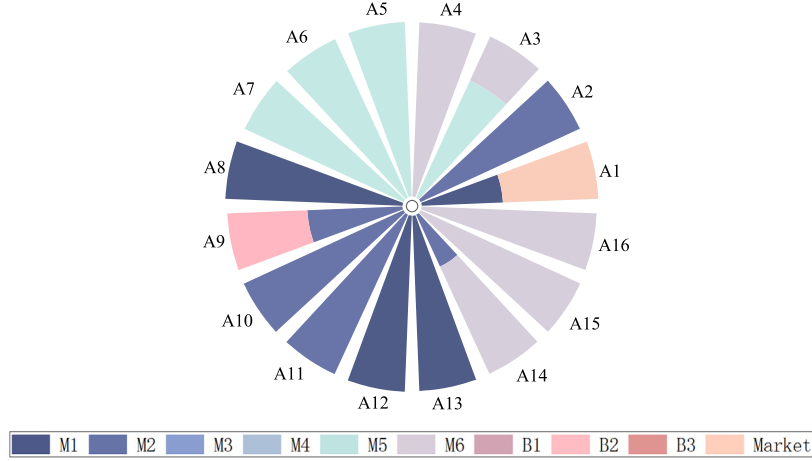


Fig. 3. Procurement strategies of the DDRO model.

to the entire battery production. The design of an RSCN can reduce the risk of production interruptions, improve production efficiency, and enhance cost-effectiveness. However, the uncertainty and seasonality in the demand for new energy vehicles result in challenges in accurately forecasting manufacturers' demand for electrolytes. We employ the proposed DDRO model to design a resilient electrolyte SC network while considering uncertain demand.

We consider the production bases of FinDreams Battery to act as buyers. Each production base has three procurement options: (i) entering into long-term contracts with primary suppliers, which offer favorable pricing but may be subject to supply disruptions; (ii) signing option contracts to reserve the right to purchase from backup suppliers; and (iii) purchasing directly from the spot market at prevailing prices. Considering geographical advantages and resource distribution, we consider 16 production bases, 6 potential primary suppliers, and 3 potential backup suppliers in the RSCN design under investigation. Their locations are illustrated in Fig. 2, and the distances among them (acquired from Baidu Maps) are summarized in Table C.1. Procurement costs are assumed to consist of raw material and transportation expenses, where the latter is calculated based on distance. Additionally, production bases can invest in improving the reliability of primary suppliers through disruption prevention measures. The values and configurations of relevant parameters used in this case are provided in Table C.2.

## 6.2. Benefits of our proposed DDRO model

Without loss of generality, we set  $\theta = 0.05, C^0 = 49\,000\,000, \varepsilon = 0.3, J = 1000$  for the experimental analysis in this section.

The computational results of the proposed DDRO model based on the SVC technique are as follows: the optimal objective value is 543 352 122.21 CNY. The selected primary suppliers are  $M1, M2, M5$ , and  $M6$ , and the selected backup supplier is  $B2$ . The warning level of the chosen primary suppliers is  $L3$ . The detailed procurement strategy is illustrated in Fig. 3.

In the proposed DDRO model, we construct a data-driven uncertainty set based on SVC technique to characterize the uncertain demand. When the demand is assumed to be precisely known, our model reduces to deterministic model (4). The optimal objective value of the deterministic model amounts to 475 173 933.19 CNY. The primary suppliers  $M1, M2, M6$  and the backup suppliers  $B1, B2$  are selected, and the warning level of these primary suppliers is  $L3$ . Under this decision, the production base does not procure from the spot market. The detailed procurement strategy is depicted in Fig. 4(a). Furthermore, we employ a budgeted uncertainty set to describe the uncertain demands;

that is, we develop the BRO model (D.3), which is presented in Appendix D. The optimal objective value amounts to 639 336 284.84 CNY. The primary suppliers  $M1, M2, M4, M5, M6$  and the backup supplier  $B2$  are selected. The warning level of the selected primary suppliers is  $L3$ . The corresponding procurement strategy is illustrated in Fig. 4(b).

As shown in Figs. 3 and 4, the optimal procurement decisions generated by the DDRO model, the deterministic model, and the BRO model are significantly different. These models select distinct sets of primary suppliers, and their approaches to market procurement also vary considerably. The deterministic model exhibits the best economic performance, whereas the BRO model is associated with the highest cost, with the DDRO model falling in between. Our robust model incurs a robust price (RP), which we evaluate using the following formula,

$$RP = \frac{Obj_R - Obj_D}{Obj_D},$$

where “ $Obj_R$ ” and “ $Obj_D$ ” indicate the optimal objective values of the RO and deterministic models, respectively. Based on this definition, the proposed DDRO model has an RP of 14.3%, compared to 34.5% for the BRO model. This indicates that the DDRO model achieves robustness at a cost that is 20.2% lower than that of the BRO model.

We conduct out-of-sample performance tests on the three optimization models to further evaluate their comparative effectiveness. The out-of-sample performance is assessed using the violation probability (VP) of constraints, which is defined as follows:

$$VP = \frac{1}{N'} \sum_{n \in N'} \left( \sum_{k \in K} \sum_{a \in A} \left( \sum_{m \in M} Y_{ma} + \sum_{b \in B} V_{ba}^k + G_a^k < d_a^k(n) \right) \right),$$

where  $N'$  denotes the number of simulation samples,  $d(n)$  represents the  $n$ th realization of the uncertain parameter  $d$ , and  $Y, V, G$  are derived from the optimal decisions of each model. We conduct 2000 independent simulation experiments. In each experiment, the cardinality of the simulated dataset is set to 100. Fig. 5 presents the probability density of  $VP$ . It can be observed that the  $VP$  of the deterministic model is significantly higher than those of the proposed DDRO and BRO models, among which the  $VP$  of the BRO model is slightly lower than that of the DDRO model. In over half of the cases, minor fluctuations in the parameters cause the optimal solution of the deterministic model to become suboptimal or even infeasible. In contrast, the BRO and DDRO models better hedge against parameter uncertainty. Moreover, we observe that the  $VP$  of the BRO model is consistently very close to zero, indicating an overly conservative behavior. This observation aligns with our earlier conclusion that the BRO model is more costly compared to the proposed DDRO model. Our DDRO model, which is proposed based on SVC technique, not only demonstrates robustness against demand uncertainty but also maintains a relatively low RP.

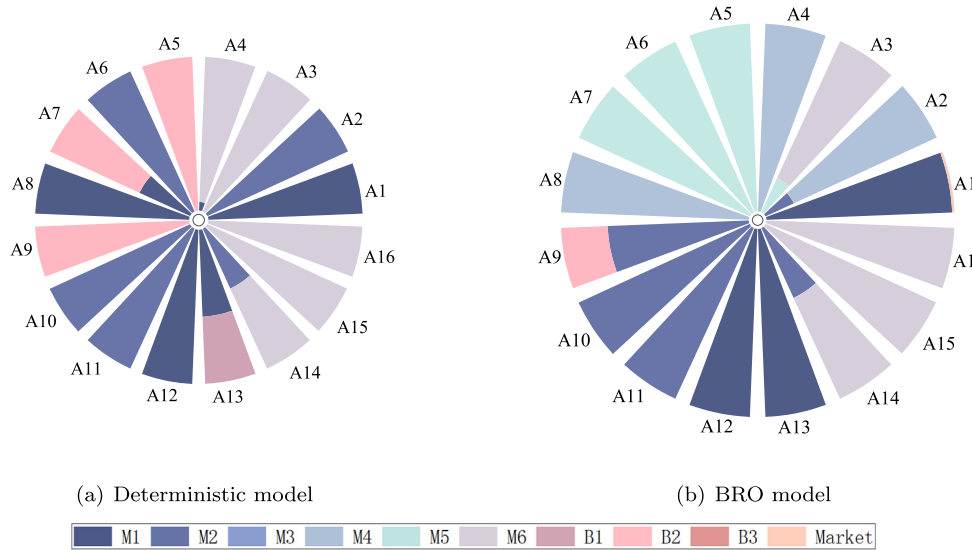


**Fig. 4.** Procurement strategies of the deterministic and BRO models

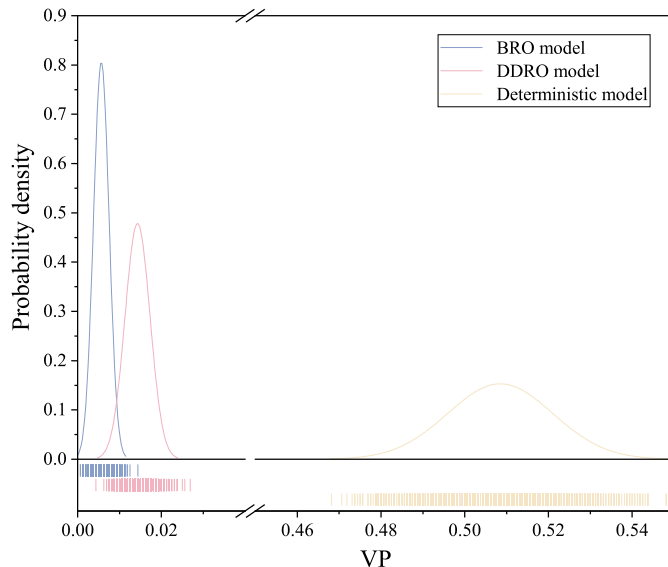


**Fig. 5.** Out-of-sample performances of different models.

### *6.3. Necessity of diversified procurement*

Following the parameter settings in Section 6.2, we conduct a study of the RSCN design under a single supplier, aiming to investigate sole sourcing decisions. Specifically, based on the diversified procurement DDRO model (19), we introduce the single supplier constraint  $\sum_{m \in M} X_m = 1$  and remove the option of backup suppliers. The resulting model, however, is found to be infeasible. Upon investigation, this infeasibility is attributed to the violation of the risk constraint of the excess probability, indicating that sole sourcing fails to meet decision-makers' expectations regarding risk aversion. To address this issue, we reset the value of  $\epsilon$  to 1, and the updated results are as follows. The optimal objective value is 587 400 869.68 CNY. The primary supplier *M6* fulfills part of the demand while the remaining portion is procured from the spot market. The warning level of the selected primary suppliers is *L3*. The specific procurement circumstances are depicted in Fig. 6. Our findings reveal that under the sole sourcing strategy, a significant portion of the demand is met through the spot market, where prices are relatively high. Compared with the diversified procurement strategy,

the production base incurs higher costs under sole sourcing. Moreover, should the sole supplier experience disruptions, the production base would face a critical situation of fulfilling all demand exclusively through the spot market.

Inspired by the observation that the sole sourcing model is infeasible when  $\varepsilon = 0.3$  and  $C^0 = 49\,000\,000$ , we examine the value of  $\text{Cost}^k$  under the sole and diversified procurement strategy. Across various  $\theta$  settings, we solve the models under each strategy, and the pertinent results are presented in [Table 3](#). As shown in the table, the diversified procurement strategy results in lower total costs compared to sole sourcing. Furthermore, by comparing the minimum and maximum value of  $\text{Cost}^k$ , it is discovered that under the diversified procurement strategy, compared to the sole sourcing strategy, the costs across different potential disruption scenarios are not only lower but also exhibit a smaller variation range. This reduced cost volatility helps mitigate investment risks for buyers, supports more accurate financial planning and budget control, and aligns better with their risk-averse decision-making preferences.

#### 6.4. Effects of risk preference

Our proposed model establishes two objectives: minimizing cost and minimizing risk. The trade-off relationship between these two objectives is illustrated through the Pareto front graph, as shown in Fig. 7. As depicted in the figure, an inverse relationship between the two objectives is identified, which provides significant insights for decision-makers when weighing cost and risk. In real-world investment and decision-making, managers consistently regard cost and risk as critical performance indicators. While reducing costs enhances profitability, lowering risk contributes to the stability of assets and operations. However, a reduction in cost often comes at the expense of increased risk and vice versa. This inherent trade-off underscores the necessity of identifying a balanced solution within the bi-objective optimization framework. The Pareto optimal frontier demonstrates how to achieve the most favorable compromise between cost and risk under given resource constraints. Each Pareto optimal solution represents a trade-off point where improving one objective cannot be achieved without compromising the other. The presence of such trade-off points enables us to identify an optimal decision-making plan, thereby achieving effective bi-objective optimization.

In light of the results from the aforementioned experiments, we further adjusted the parameter  $C^0$  within the DDRO model to strengthen the decision-maker's risk-averse posture and examine the corresponding decision-making behavior under this new setting. The computational results of the model are presented as follows. The optimal

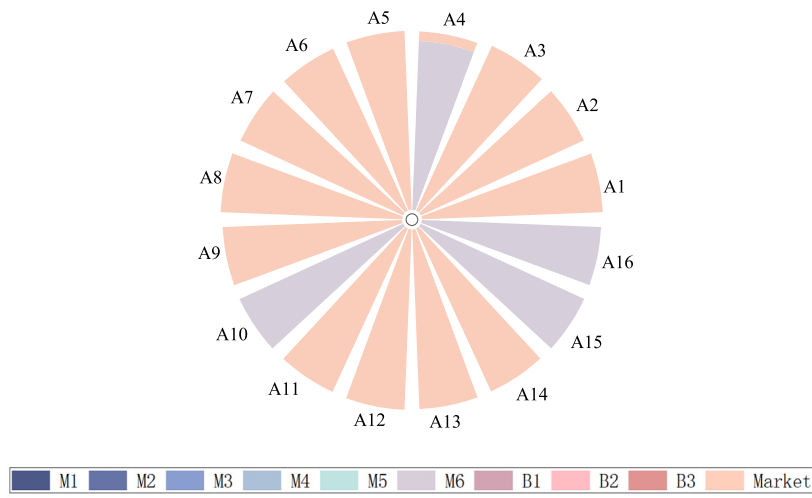


Fig. 6. Procurement strategies of the sole sourcing model.

Table 3

The pertinent outcomes of the models under diverse procurement strategies.

Procurement strategy	$\theta = 0.02$				$\theta = 0.08$				$\theta = 0.14$										
	Optimal objective value	Cost <sup>k</sup>		Optimal objective value	Cost <sup>k</sup>		Optimal objective value	Cost <sup>k</sup>		Optimal objective value	Cost <sup>k</sup>								
		Minimum	Maximum		Minimum	Maximum		Minimum	Maximum		Minimum	Maximum							
Sole	589 680 366.99	515 263 290.68	416 265 552.06	585 105 180.75	510 189 778.39	412 166 815.68	582 998 886.23	507 866 974.68	41 029 029.316	Diversified	545 552 776.94	32 623 837.67	28 060 260.54	541 124 478.02	29 858 442.84	25 509 589.16	539 088 313.95	28 349 277.27	24 178 777.49

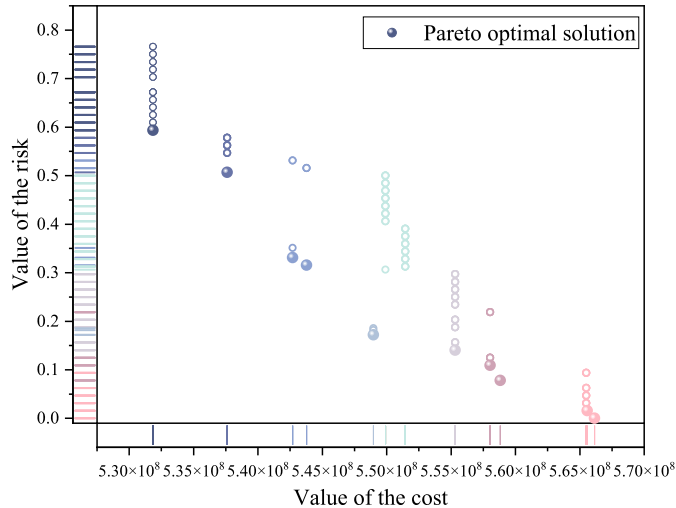


Fig. 7. The Pareto front of the bi-objective optimization problem.

objective value is 586 166 725.79 CNY. The selected primary suppliers include  $M_1$ ,  $M_2$ ,  $M_3$ ,  $M_4$ , and  $M_6$ , with warning levels  $L_2$ ,  $L_3$ ,  $L_3$ ,  $L_3$ , and  $L_3$ , respectively. The detailed procurement strategies are illustrated in Fig. 8. This figure presents a grouped bar chart, where each category contains two bars, comparing procurement strategies under  $C^0 = 49\ 000\ 000$  and  $C^0 = 9\ 000\ 000$ . Each buyer's procurement strategy is represented by two adjacent vertical bars: the left bar corresponds to  $C^0 = 49\ 000\ 000$  (consistent with Fig. 3), and the right bar represents  $C^0 = 9\ 000\ 000$ . We discover that the optimal decision at this juncture undergoes a marked change, which indicates the significant impact of decision-makers' risk preferences, and risk-averse managers prioritize stable supply bases over cost minimization.

Table 4

Probability of exceeding the budget level in solutions optimized by different indicators.

Indicators	Budget level				
	18 800 000	18 925 000	19 050 000	19 175 000	19 300 000
CVaR	100.00%	79.69%	56.25%	34.38%	9.38%
EPF( $C^0 = 18\ 900$ )	25.00%	0.00%	0.00%	0.00%	0.00%
EPF( $C^0 = 19\ 000$ )	46.88%	18.75%	0.00%	0.00%	0.00%
EPF( $C^0 = 19\ 100$ )	70.31%	43.75%	14.06%	0.00%	0.00%
EPF( $C^0 = 19\ 200$ )	81.25%	57.81%	35.94%	6.25%	0.00%

### 6.5. Comparison of EPF and CVaR indicators

The CVaR is a commonly used indicator for quantifying risk aversion that measures the expected cost exceeding a certain confidence level (Value at Risk), which is defined as follows,

$$\text{CVaR}_\eta = E_p[\text{Cost}(X, Y, Q, Z; k) | \text{Cost}(X, Y, Q, Z; k) > \text{VaR}_\eta],$$

where  $\text{VaR}_\eta$  denotes the  $\eta$ -quantile of the cost distribution (Rockafellar and Uryasev, 2002). To provide a comprehensive evaluation of how different risk measurement approaches influence decision outcomes, we compute the CVaR-objective model under the same parameter settings as those used in Section 6.2. The model yields a total cost of 543 445 254.48 CNY, and the corresponding procurement strategies are presented in Fig. 9. These results exhibit significant differences compared to those obtained from the EPF model.

Notably, the CVaR and EPF represent two distinct perspectives on risk assessment. The CVaR focuses on tail risk, offering decision-makers cost guarantees under extreme scenarios. It quantifies the degree of risk exposure in extreme situations through the conditional expectation beyond a specified threshold (Rockafellar and Uryasev, 2002). In contrast, the EPF indicator concentrates on the probability of exceeding a specific threshold, making it more appropriate for decision-makers with threshold-sensitive risk aversion—they prioritize ensuring that costs do not exceed preselected thresholds (Schultz and Tiedemann, 2003). To

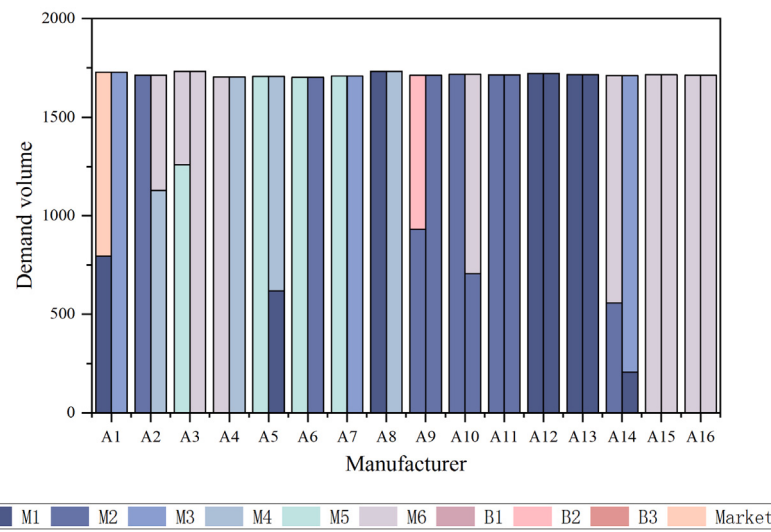


**Fig. 8.** Comparison of procurement strategies in the DDRO model under parameter  $C^0 = 49\,000\,000$  vs.  $C^0 = 9\,000\,000$ .

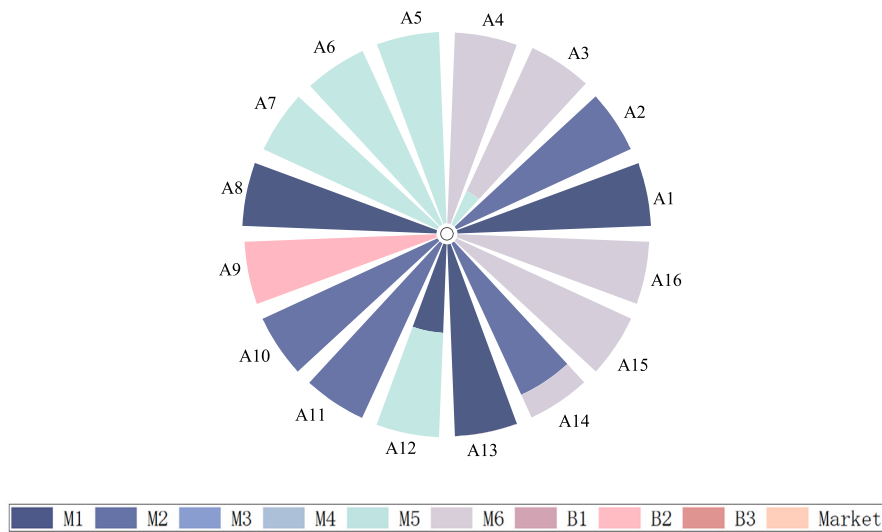


**Fig. 9.** Procurement strategies of the model with CVaR indicator.

evaluate the relative effectiveness of the EPF indicator over the CVaR in threshold-sensitive decision contexts, we conduct a comprehensive experiment under the same cost constraints. Results, summarized in [Table 4](#), demonstrate that SC optimal solutions using the EPF indicator consistently maintain lower probabilities of budget exceedance than those determined by the CVaR indicator. These findings support our theoretical claim that the EPF provides more effective risk management for SC decision-makers whose primary concern is maintaining costs below budget thresholds. By directly targeting exceedance probability, the EPF aligns more closely with threshold-oriented risk preferences, thereby providing a more tailored and effective framework for managing risk in budget-constrained operations where threshold violations entail significant consequences.

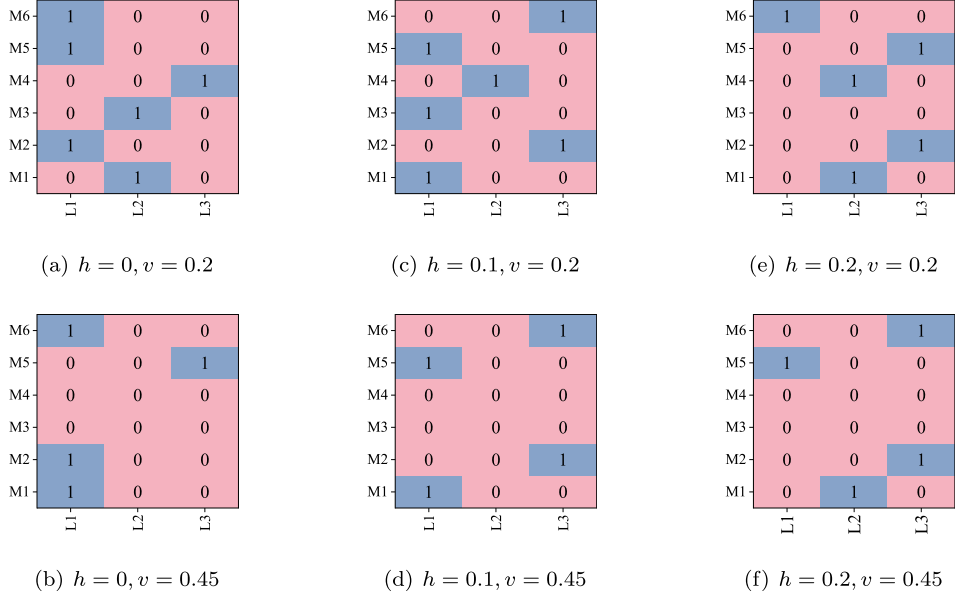
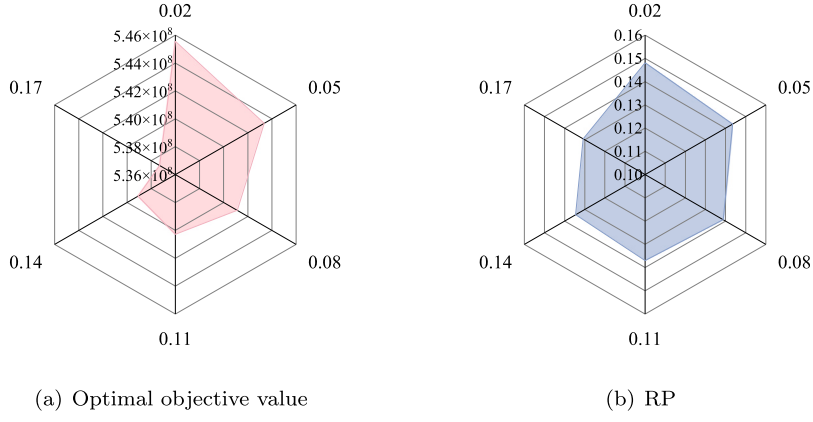
Our experimental results demonstrate that different risk measures lead to different decision outcomes, highlighting the importance of selecting appropriate risk indicators in risk-averse decision modeling and providing empirical support for model selection under varying risk preferences. While the CVaR is better suited for decision-makers who prioritize the mitigation of extreme losses, the EPF proves more effective for those aiming to minimize budget overruns, typically ensuring greater cost control. Therefore, the EPF indicator is a better choice

in SC management as it helps in cost optimization and financial risk reduction.

## 6.6. Sensitivity analysis

### 6.6.1. Sensitivity analysis of the $v$ and $h$

Given the significance of suppliers' warning and recovery capabilities, we conduct a sensitivity analysis on the parameters  $v$  and  $h$  representing them. [Table 5](#) presents the optimal objective value of the model under diverse settings of  $v$  and  $h$ . As shown in the table, when the recovery rate is zero, the model fails to yield a feasible solution. This may be attributed to the lack of an effective feedback mechanism for coping with SC disruptions in the absence of a recovery capability. This observation strongly supports the necessity for buyers to invest efforts in improving suppliers' recovery rates. Moreover, as the recovery rate increases gradually, suppliers demonstrate enhanced recovery capabilities, indicating a stronger ability to manage potential risks or disruptions, thereby mitigating the impact of SC disruptions. This brings about a reduction in the total cost since a higher recovery rate implies fewer losses and delays, thereby enhancing the efficiency and reliability of the SC. The improvement in warning capabilities suggests that suppliers are better equipped to detect potential issues

Fig. 10. The optimal effort decisions under various  $v$  and  $h$ .Fig. 11. Radar graph of the optimal objective value and RP under different  $\theta$ .

**Table 5**  
The optimal objective value of the model under diverse settings of  $v$  and  $h$ .

$h$	$v$		
		0	0.2
0	Infeasible	686 724 404.75	573 885 875.34
0.1	Infeasible	678 360 572.30	560 234 600.67
0.2	Infeasible	647 450 487.21	543 332 611.62

in a timely manner and take preemptive actions to avoid or minimize their consequences. We further analyze the optimal effort decisions of the model under different recovery rates and warning capabilities, as illustrated in Fig. 10. Our findings reveal that variations in recovery rates and warning capabilities lead to differences in the optimal solutions. This might be attributed to the possibility that they bring about alterations in the overall operational mode and efficiency of the SC.

#### 6.6.2. Sensitivity analysis of the $\theta$

Figs. 11(a) and 11(b) respectively depict the radar diagrams of the optimal objective value and RP of the DDRO model under different sizes of the uncertainty set. As shown in Fig. 11, both the optimal objective value and RP exhibit a decreasing trend as  $\theta$  increases.

This can be explained by the fact that the data-driven uncertainty set based on SVC gradually shrinks with increasing  $\theta$ , while the optimal objective value and RP are calculated based on the worst-case principle. Consequently, the observed decline in both metrics is reasonable. To further compare the out-of-sample performance of the DDRO model under different sizes of uncertainty sets, we select the cases of  $\theta = 0.05$  and  $\theta = 0.1$  as examples and plot the frequency distribution of  $VP$ , as illustrated in Fig. 12. It can be observed that when  $\theta = 0.05$ , the data-driven uncertainty set is larger than when  $\theta = 0.1$ , leading to a more conservative setting and thus producing a lower  $VP$ . Our findings are consistent with theoretical expectations.

#### 6.6.3. Sensitivity analysis of the $J$

The demand data quantity used in the above numerical experiments is 1000. We analyze the model with varying data quantities to investigate the impact of data volume on model performance. Illustrated in Fig. 13, when  $\theta = 0.07$ , the optimal objective value gradually decreases from 591 747 886.38 CNY to 545 386 377.22 CNY as the data volume rises from 200 to 1400. Similarly, with  $\theta = 0.01$  and 0.13, the optimal objective value diminishes with increasing data volume. This indicates that an increased data volume enables decision-makers to derive more accurate optimal solutions at a lower cost. However, this improvement

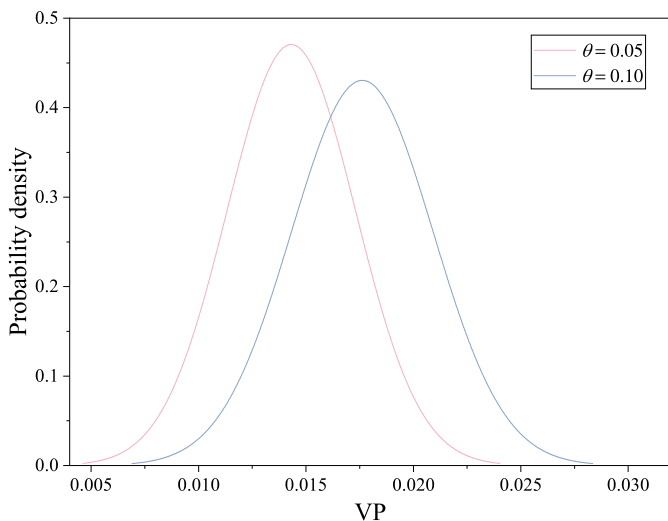


Fig. 12. Out-of-sample performances of DDRO model under different  $\theta$ .

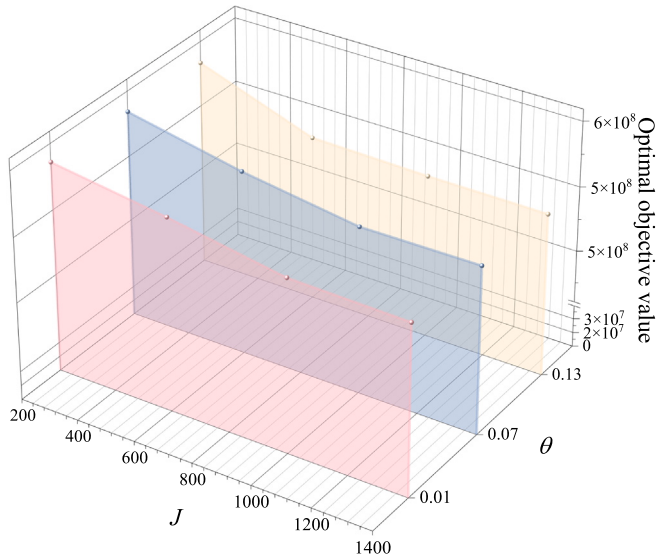


Fig. 13. Optimal objective values in the context of diverse data volumes.

is not uniformly distributed. Take  $\theta = 0.07$  as an example, the most substantial cost reduction of 4.8% occurs in the initial data expansion from 200 to 600 points. The subsequent improvement from 600 to 1000 points yields a 3.6% reduction, while further expansion to 1400 points delivers only an additional 0.2% improvement. This pattern is consistently observed across all  $\theta$  tested values. Our analysis further identifies a critical threshold effect of around 1000 data points, beyond which additional data collection yields marginally diminishing benefits. This threshold appears consistent across different uncertainty parameters, suggesting it may represent a fundamental property of the data-driven modeling approach rather than being parameter-dependent. These findings carry important implications for practical implementation. They suggest that decision-makers should prioritize collecting sufficient quality data (approximately 1000 points in our case study) rather than pursuing excessive data collection. Beyond this threshold, resources might be better allocated to other aspects of SC optimization rather than continued data acquisition efforts.

## 6.7. Theoretical and practical implications

From our comprehensive experimental results, we obtain key implications that advance both theoretical understanding and practical application of our RSCN design.

**Theoretical implications:** (i) Optimization method: Compared with the traditional BRO method, our DDRO approach achieves a balance between uncertainty handling and cost efficiency, indicating that utilizing historical data through the SVC technique can reduce conservatism while preserving robustness. (ii) Risk-cost trade-off framework: Our bi-objective optimization model generates a Pareto frontier that can empirically verify the inverse relationship between risk and cost, providing a mathematical framework for analyzing these complex trade-offs. (iii) Risk measure performance: Our EPF indicator has a measurable advantages over the CVaR indicator in threshold-sensitive scenarios, enhancing our theoretical understanding of risk measure selection in SC optimization. (iv) Non-linear returns: The improvement objective value follows a non-linear trajectory, and when the amount of collected data exceeds a certain threshold a decrease in returns is observed, which confirms the theoretical predictions of information values in complex systems.

**Practical implications:** (i) Uncertainty management: It is recommended that decision-makers adopt our DDRO approach when historical data are available, compared to the BRO approach, it can not only deliver significant cost savings but also effectively mitigate uncertainty. (ii) Risk preference alignment: Decision-makers should explicitly define their risk preferences, and use our Pareto frontier to select solutions that can align with their priorities before designing SCs. Under strict budget constraints, our EPF indicator can provide excellent control by minimizing the probability of exceeding risk thresholds. (iii) Investment prioritization: In case of limited budget, recovery capability is a critical prerequisite, while investments in early warning capability show diminishing returns. Data collection efforts should prioritize quality and adequacy over pure quantity. (iv) Procurement strategy: In a risk-averse environment, diversified procurement always outperforms sole sourcing, achieving lower costs and greater resilience during disruptions.

These implications bridge theoretical advancement and practical application, providing both academic contributions to optimization theory and actionable insights for decision-makers facing complex RSCN design decisions in uncertain environments.

## 6.8. Managerial insights of our work

In this work, several managerial insights can be summarized that provide quantitative evidence, reveal complex trade-offs, and offer practical frameworks to guide decision-making in RSCN design.

Firstly, uncertainty is inevitable in practical applications, and neglecting it may lead to serious consequences, as fluctuations in model parameters may result in suboptimal or even infeasible solutions. Our comparative analysis reveals that our data-driven approach achieves a balance point in the risk-cost spectrum when demands are uncertain, and some historical data information is available. Specifically, the robustness cost of our DDRO model is lower than that of the BRO model. This quantitative advantage demonstrates that properly leveraging historical data through SVC techniques can significantly reduce conservatism without compromising robustness. This practical implication equates to substantial cost savings.

Secondly, decision-makers' risk preferences significantly impact the solution results. Our experiments reveal that cost and risk are inversely related, and achieving simultaneous minimization is challenging. The Pareto frontier generated by our bi-objective optimization model provides a concrete decision-making framework for trade-offs. Decision-makers can select solutions on the frontier that align with their priorities. Furthermore, our comparison of risk measures focusing on two perspectives, EPF and CVaR, highlights the importance of

selecting appropriate risk measures. The EPF offers advantages over commonly used the CVaR approaches for threshold-sensitive decision-makers. The EPF enhances budget control by minimizing threshold exceedance probability and reducing financial risk exposure. Our experiments confirm that EPF-optimized solutions consistently outperform the CVaR optimized solutions in maintaining lower threshold exceedance probabilities. This approach benefits decision-makers facing strict budgetary constraints or severe consequences for cost overruns.

Finally, we examine the influence of key model parameters on the optimal solutions and their objective values. Supplier recovery capability becomes an indispensable prerequisite in RSCN design within specific budget constraints. Warning capability investment exhibits diminishing returns relative to recovery capability. Moreover, the diversified procurement strategy proves superior in risk-averse contexts. Compared to sole-sourcing procurement, multi-sourcing procurement reduces costs and exhibits a higher cost stabilization effect in disruption scenarios, making it valuable for risk-averse decision-makers. Additionally, our analysis reveals that optimal objective value improvements follow a non-linear trajectory as data volume increases, with diminishing returns beyond certain thresholds. This suggests that decision-makers should focus on collecting high-quality, sufficient data rather than maximizing quantity.

These insights provide decision-makers with quantified, actionable guidance that offers specific strategic priorities and a robust framework for resilient SC design in practical settings.

## 7. Conclusions

Considering that supply disruptions are often associated with significant financial losses and buyers typically adopt risk-averse strategies as a means of mitigation, this paper developed an RSCN that incorporates diversified procurement and disruption prevention strategies for risk-averse decision-makers. Specifically, we considered three procurement sources: primary suppliers, backup suppliers, and spot markets, while allowing buyers to invest in efforts aimed at improving suppliers' warning and recovery capabilities to mitigate the impact of disruptions. We quantified decision-makers' risk preferences using the EPF indicator and incorporated these preferences into the model through the epsilon-constraint method, which enabled decision-makers to balance risk and cost effectively. Given the inherent uncertainty in real-world environments, we accounted for uncertain demand patterns. These uncertainties are captured through an SVC-based data-driven uncertainty set, based on which we constructed a DDRO model. Leveraging cone duality theory, we reformulated the original model into a computationally tractable MILP algebraic system and designed a BD algorithm to solve it. Finally, we validate the effectiveness and superiority of the proposed DDRO model through a real-world case study involving the electrolyte SC of FinDreams Battery. The key findings of this paper are summarized as follows:

- By comparing our DDRO model with the deterministic and BRO models, the experimental results demonstrate our model's favorable effect and economic benefit in resisting uncertain demand.
- By adjusting the regularization parameters, the size of the uncertainty set can be controlled, which is related to the decision-maker's degree of conservatism. The larger the regularization parameter, the weaker the robustness of the obtained optimal solution.
- The risk-averse preferences of decision-makers significantly impact decision-making. Decision-makers need to balance costs and risks. Our EPF indicator has an advantage over CVaR in controlling budget overruns.
- The diversified procurement and disruption prevention contribute to economical and resilient SCs. Buyers' efforts in both areas are essential.

- The quantity of historical data for uncertain demands is crucial, and an appropriately sized dataset typically enables decision-makers to obtain a more accurate solution.

Future research directions can extend our work in several important dimensions. Firstly, we focused exclusively on the critical uncertain demand parameter, without incorporating its distribution information into our discussion. Secondly, developing advanced disruption propagation models that account for simultaneous or cascading failures across both primary and backup suppliers would deepen our understanding of complex SC disruptions. Finally, studying the optimal balance between reliability investment and supplier diversification under joint disruption scenarios will provide implementable insights for decision-makers.

## CRediT authorship contribution statement

**Yanjiao Wang:** Writing – original draft, Software, Methodology, Data curation, Conceptualization, Validation. **Aixia Chen:** Writing – review & editing, Methodology, Conceptualization, Visualization. **Naiqi Liu:** Writing – review & editing, Funding acquisition, Project administration.

## Declaration of competing interest

The authors declare that they have no known competing financial interests or personal relationships that could have appeared to influence the work reported in this paper.

## Acknowledgments

Yanjiao Wang and Aixia Chen contributed equally to this work. The authors gratefully acknowledge the insightful comments received from the Editor-in-Chief, Editor Ou Tang and anonymous reviewers for their constructive comments, which have considerably improved the quality of the paper. This work was supported by the Natural Science Foundation of Hebei Province (No. A2023201020), the Operations Research and Management Innovation Team of Hebei University, China (No. IT2023C02), the National Natural Science Foundation of China (Nos. 61773150, 72471164), and the Postgraduate's Innovation Fund Project of Hebei Province (CXZZSS2025002).

## Appendix A. Notations and definitions

See Table A.1.

## Appendix B. Proof of Theorem 1

For the convenience of derivation, we reformulate constraint (24c) as follows,

$$\sum_{m \in M} Y_{ma} + \sum_{b \in B} V_{ba}^k + G_a^k \geq \max_{d^k \in \mathcal{U}(\mathcal{D}^k)} \sum_{a' \in A} d_{a'}^k E_{a'a}^k \quad \forall k \in K, \forall a \in A, \quad (\text{B.1})$$

where  $E^k \in R^{|A| \times |A|}$  is an identity matrix.

Leveraging transformed form (25) of uncertainty set (18), the right-hand side of constraint (B.1) can be presented as follows ( $\forall k \in K, \forall a \in A$ ),

$$\max_{d^k, \Psi^k} [d^k]^T e^{ak} \quad (\text{B.2a})$$

$$\text{s.t. } \sum_{j \in SV^k} \alpha_j^k (\Psi_j^k)^T \mathbf{1} \leq \tau^k, \quad (\text{B.2b})$$

$$-\Psi_j^k \leq \bar{Q}^k (d^k - d^k(j)) \quad \forall j \in SV^k, \quad (\text{B.2c})$$

$$\bar{Q}^k (d^k - d^k(j)) \leq \Psi_j^k \quad \forall j \in SV^k, \quad (\text{B.2d})$$

where  $e^{ak}$  is the  $a$ th column of the matrix  $E^k$ .

**Table A.1**  
Notations and definitions.

Notations	Definitions
Sets	
$A$	Set of buyers;
$B$	Set of potential backup suppliers;
$K$	Set of potential disruption scenarios;
$L$	Set of buyer's effort level;
$M$	Set of potential primary suppliers.
Parameters	
$c_m$	Capacity of primary supplier $m$ ;
$d_a$	Demand of buyer $a$ ;
$f_m$	Fixed cost of a contract with primary supplier $m$ ;
$g_{ml}$	Costs incurred in the buyer's effort level $l$ to improve the supplier's warning capability;
$h_{ml}$	The warning ability of supplier $m$ in the event of an effort level $l$ from the buyer;
$i_m^k$	1 if primary supplier $m$ is affected by scenario $k$ ; 0 otherwise;
$N$	A large number;
$n_m^k$	Capacity residual rate of primary suppliers experiencing outages under scenario $k$ ;
$o_{ba}$	Purchase price from backup supplier $b$ for buyer $a$ ;
$p^k$	Probability of scenario $k$ occurring;
$q^k$	Market price under scenario $k$ ;
$r_b$	Reserve cost per unit capacity of backup supplier $b$ ;
$s_{ma}$	Purchase price from primary supplier $m$ for buyer $a$ ;
$t^{max}$	Maximum allowable recovery period that the buyer is willing to tolerate;
$v_{ml}$	Recovery rate per unit time of primary supplier $m$ at level $l$ .
Decision variables	
$G_a^k$	Amount purchased by buyer $a$ from the market under scenario $k$ ;
$Q_b$	Reserved capacity of backup supplier $b$ ;
$T_m^k$	Permitted recovery duration for primary supplier $m$ following an interruption under scenario $k$ ;
$V_{ba}^k$	Supply from backup supplier $b$ to buyer $a$ under scenario $k$ ;
$X_m$	1 if primary supplier $m$ is selected, 0 otherwise;
$Y_{ma}$	The volume of supply from primary supplier $m$ to buyer $a$ ;
$Z_{ml}$	1 if the buyer exerts effort at level $l$ to enhance the warning capability of supplier $m$ .

Introducing dual variables  $\Omega^{ak}, Y_j^{ak}, \Gamma_j^{ak}$  for constraints (B.2b) – (B.2d), respectively, the dual of model (B.2) is presented as follows,

$$\min_{\Omega^{ak}, Y_j^{ak}, \Gamma_j^{ak}} \sum_{j \in SV^k} (\Gamma_j^{ak} - Y_j^{ak})^T \bar{Q}^k d^k(j) + \Omega^{ak} \tau^k \quad (B.3a)$$

$$\text{s.t. } \sum_{j \in SV^k} \bar{Q}^k (Y_j^{ak} - \Gamma_j^{ak}) + e^{ak} = \mathbf{0}, \quad (B.3b)$$

$$Y_j^{ak} + \Gamma_j^{ak} = \Omega^{ak} \alpha_j^k \mathbf{1} \quad \forall j \in SV^k, \quad (B.3c)$$

$$Y_j^{ak}, \Gamma_j^{ak} \in R_+^{|A|}, \Omega^{ak} \in R_+ \quad \forall j \in SV^k. \quad (B.3d)$$

In the case  $0 < \theta < 1$ , strong duality holds between primal problem (B.2) and its dual problem (B.3). Thus, semi-infinite constraint (24c) is transformed into the following tractable linear system,

$$\sum_{m \in M} Y_{ma} + \sum_{b \in B} V_{ba}^k + G_a^k \geq \sum_{j \in SV^k} (\Gamma_j^{ak} - Y_j^{ak})^T$$

$$\times \bar{Q}^k d^k(j) + \Omega^{ak} \tau^k \quad \forall k \in K, \forall a \in A,$$

$$\sum_{j \in SV^k} \bar{Q}^k (Y_j^{ak} - \Gamma_j^{ak}) + e^{ak} = \mathbf{0} \quad \forall k \in K, \forall a \in A,$$

$$Y_j^{ak} + \Gamma_j^{ak} = \Omega^{ak} \alpha_j^k \mathbf{1} \quad \forall j \in SV^k, \forall k \in K, \forall a \in A,$$

$$Y_j^{ak}, \Gamma_j^{ak} \in R_+^{|A|}, \Omega^{ak} \in R_+ \quad \forall j \in SV^k, \forall k \in K, \forall a \in A.$$

## Appendix C. Experimental data

See Tables C.1 and C.2.

## Appendix D. BRO model for the RSCN design problem

In this section, we develop a budgeted uncertainty set for the RSCN design problem and establish the BRO model under this uncertainty set.

**Construction of budgeted uncertainty set.** Assume that the demand  $d^k$  is depicted by the following budgeted uncertainty set,

$$\mathcal{U}(\mathcal{D}^k)_{\text{Budgeted}} = \left\{ d^k \in R^{|A|} \mid d_a^k = \bar{d}_a^k + \sum_{i \in I} \zeta_i^k \Delta d_a^k(i), \forall a \in A : \zeta \in \mathcal{Z}^k \right\}, \quad (D.1)$$

where  $\bar{d}^k$ ,  $\Delta d^k$ , and  $\zeta^k$  denote the nominal value, the basic shift and the perturbation vector of  $d$ , respectively, and  $\mathcal{Z}^k$  is the perturbation set,

$$\mathcal{Z}^k = \left\{ \zeta^k \in R^I \mid \|\zeta^k\|_\infty \leq 1, \|\zeta^k\|_1 \leq \sigma^k \right\}, \quad (D.2)$$

where  $\sigma^k = \sqrt{2 \times \log(1/\theta_k)}$ , and  $\theta_k$  is the regularization parameter employed to control the magnitude of the budgeted uncertainty set.

**Formulation of BRO model.** Based on constructed budgeted uncertainty set  $\mathcal{U}(\mathcal{D}^k)_{\text{Budgeted}}$  (D.1), we formulate the following BRO model for the RSCN design problem,

$$\min_{X, Y, Q, Z, V, G} \text{Obj}^1(X, Y, Q, Z, V, G) \quad (D.3a)$$

$$\text{s.t. } \text{Obj}^{2'}(X, Y, Q, Z, V, G, \rho) \leq \varepsilon, \quad (D.3b)$$

$$\sum_{m \in M} Y_{ma} + \sum_{b \in B} V_{ba}^k + G_a^k \geq \max_{d^k \in \mathcal{U}(\mathcal{D}^k)_{\text{Budgeted}}} d_a^k \quad \forall k \in K, \forall a \in A, \quad (D.3c)$$

$$\text{Constraints (1a), (3c), (3e) – (3g), (20), (21), (22b), (22c).} \quad (D.3d)$$

**Derivation of robust counterpart.** The presence of semi-infinite constraint (D.3c) renders model (D.3) a computationally intractable model. Below, we deduce the tractable robust counterpart form of model (D.3).

Based on the structure of perturbation set (D.2), semi-infinite constraint (D.3c) can be expressed as the following tractable system with variables  $\Theta$ ,  $\Xi \in R^{I \times |A| \times |K|}$ :

$$\begin{aligned} \sum_{m \in M} Y_{ma} + \sum_{b \in B} V_{ba}^k + G_a^k &\geq \sum_{i \in I} |\Theta_i^{ak}| \\ &+ \sigma^k \max_{i \in I} |\Xi_i^{ak}| + [\bar{d}^k]^T e^a \quad \forall k \in K, \forall a \in A, \end{aligned} \quad (D.4a)$$

$$\Theta_i^{ak} + \Xi_i^{ak} = -[\Delta d^k(i)]^T e^a \quad \forall i \in I, \forall k \in K, \forall a \in A. \quad (D.4b)$$

Consequently, BRO model (D.3) is reformulated as the following tractable MILP problem,

$$\begin{aligned} \min_{X, Y, Q, Z, V, G} & \text{Obj}^1(X, Y, Q, Z, V, G) \\ \text{s.t. } & \text{Obj}^{2'}(X, Y, Q, Z, V, G, \rho) \leq \varepsilon, \\ & \text{Constraints (1a), (3c), (3e) – (3g), (20), (21), (22b), (22c), (D.4a), (D.4b).} \end{aligned} \quad (D.5)$$

## Data availability

Data will be made available on request.

**Table C.1**  
Relevant distance parameters (kilometer).

Sourcing	Production base															
	A1	A2	A3	A4	A5	A6	A7	A8	A9	A10	A11	A12	A13	A14	A15	A16
M1	1489	639	333	384	1045	404	64	623	528	522	850	777	766	1141	1454	1341
M2	2443	1991	1637	1471	2048	1430	1293	983	937	833	837	653	592	1076	854	351
M3	1841	830	652	744	814	126	371	850	714	528	1037	658	783	825	1197	1200
M4	1429	1271	878	618	1804	1117	719	168	315	613	182	838	573	1471	1567	1208
M5	400	968	828	733	1925	1468	1106	1089	1171	1425	1245	1719	1542	2221	2468	2211
M6	2602	2030	1702	1572	1962	1397	1339	1128	1053	877	1021	629	682	895	613	121
B1	1620	1514	1120	864	1987	1291	925	363	471	704	143	856	566	1505	1526	1109
B2	1492	1334	941	684	1841	1149	763	199	332	612	118	817	542	1458	1534	1160
B3	1563	1127	742	542	1531	836	479	139	14	320	316	580	372	1188	1332	1041

**Table C.2**

Distribution and value of relevant parameters in case study.

Parameter	Distribution	Parameter	Value
$f$	Uniform[55 000 000, 75 000 000]	$v$	$v_{m1} = 0, v_{m2} = 0.2, v_{m3} = 0.45$
$r$	Uniform[11 000, 13 000]	$t$	0.8
$c$	Uniform[5000, 7000]	$h$	$h_{m1} = 0, h_{m2} = 0.1, h_{m3} = 0.2$
$n$	Uniform[0.5, 0.8]	$g$	$h \times \text{Uniform}[400 000, 500 000]$
$d$	Normal(1500, 100)		

## References

- Aboytes-Ojeda, M., Castillo-Villar, K.K., Cardona-Valdés, Y., 2022. Bi-objective stochastic model for the design of biofuel supply chains incorporating risk. *Expert Syst. Appl.* 202, 117285. <http://dx.doi.org/10.1016/j.eswa.2022.117285>.
- Aghajani, M., Torabi, S.A., Altay, N., 2023. Resilient relief supply planning using an integrated procurement-warehousing model under supply disruption. *Omega* 118, 102871. <http://dx.doi.org/10.1016/j.omega.2023.102871>.
- Azad, N., Hassini, E., 2019. Recovery strategies from major supply disruptions in single and multiple sourcing networks. *European J. Oper. Res.* 275 (2), 481–501. <http://dx.doi.org/10.1016/j.ejor.2018.11.044>.
- Ben-Hur, A., Horn, D., Siegelmann, H.T., Vapnik, V., 2001. Support vector clustering. *J. Mach. Learn. Res.* 2 (Dec), 125–137.
- Ben-Tal, A., El Ghaoui, L., Nemirovski, A., 2009. Robust Optimization. Princeton University Press, Princeton.
- Chen, S., Chen, Y., 2025. Designing a resilient supply chain network: A multi-objective data-driven distributionally robust optimization method. *Comput. Oper. Res.* 173, 106868. <http://dx.doi.org/10.1016/j.cor.2024.106868>.
- Chen, S., Zhang, M., Ding, Y., et al., 2020. Resilience of China's oil import system under external shocks: A system dynamics simulation analysis. *Energy Policy* 146, 111795. <http://dx.doi.org/10.1016/j.enpol.2020.111795>.
- Chowdhury, P., Paul, S.K., Kaisar, S., Moktadir, M.A., 2021. COVID-19 pandemic related supply chain studies: A systematic review. *Transp. Res. E Logist. Transp. Rev.* 148, 102271. <http://dx.doi.org/10.1016/j.tre.2021.102271>.
- Dixit, V., Omar, A., Tang, O., Verma, P., 2024. Capacity management under uncertain demand and distribution policies: the case of Indian vaccine supply chain. *Int. J. Prod. Res.* 1–25. <http://dx.doi.org/10.1080/00207543.2024.2392625>.
- Dixit, V., Verma, P., Tiwari, M.K., 2020. Assessment of pre and post-disaster supply chain resilience based on network structural parameters with cva as a risk measure. *Int. J. Prod. Econ.* 227, 107655. <http://dx.doi.org/10.1016/j.ijpe.2020.107655>.
- Fallahpour, A., Nayeri, S., Sheikhalishahi, M., Wong, K.Y., Tian, G., Fathollahi-Fard, A.M., 2021. A hyper-hybrid fuzzy decision-making framework for the sustainable-resilient supplier selection problem: A case study of Malaysian Palm oil industry. *Env. Sci. Pollut. Res.* 1–21. <http://dx.doi.org/10.1007/s11356-021-12491-y>.
- Feng, Y., Chen, Y., Liu, Y., 2023. Optimising two-stage robust supplier selection and order allocation problem under risk-averse criterion. *Int. J. Prod. Res.* 61 (19), 6356–6380. <http://dx.doi.org/10.1080/00207543.2022.2127963>.
- Feng, Y., Liu, Y., Chen, Y., 2022. A robust multi-supplier multi-period inventory model with uncertain market demand and carbon emission constraint. *Comput. Ind. Eng.* 165, 107937. <http://dx.doi.org/10.1016/j.cie.2022.107937>.
- Fosso Wamba, S., Guthrie, C., Queiroz, M.M., Minner, S., 2024. ChatGPT and generative artificial intelligence: an exploratory study of key benefits and challenges in operations and supply chain management. *Int. J. Prod. Res.* 62 (16), 5676–5696. <http://dx.doi.org/10.1080/00207543.2023.2294116>.
- Gao, S.Y., Simchi-Levi, D., Teo, C.P., Yan, Z., 2019. Disruption risk mitigation in supply chains: The risk exposure index revisited. *Oper. Res.* 67 (3), 831–852. <http://dx.doi.org/10.1287/opre.2018.1776>.
- Goudarzi, F.S., Olaru, D., Bergey, P., 2023. Beyond risk attitude: Unpacking behavioral drivers of supply chain contracts. *Int. J. Prod. Econ.* 255, 108678. <http://dx.doi.org/10.1016/j.ijpe.2022.108678>.
- Han, B., Zhang, Y., Wang, S., Park, Y., 2023. The efficient and stable planning for interrupted supply chain with dual-sourcing strategy: a robust optimization approach considering decision maker's risk attitude. *Omega* 115, 102775. <http://dx.doi.org/10.1016/j.omega.2022.102775>.
- Hohenstein, N.O., Feisel, E., Hartmann, E., Giunipero, L., 2015. Research on the phenomenon of supply chain resilience: a systematic review and paths for further investigation. *Int. J. Phys. Distrib. Logist. Manag.* 45 (1/2), 90–117. <http://dx.doi.org/10.1108/IJPDLM-05-2013-0128>.
- Kumar, D., Soni, G., Mangla, S.K., Liao, J., Rathore, A.P.S., Kazancoglu, Y., 2024. Integrating resilience and reliability in semiconductor supply chains during disruptions. *Int. J. Prod. Econ.* 276, 109376. <http://dx.doi.org/10.1016/j.ijpe.2024.109376>.
- Li, T., Sethi, S.P., Zhang, J., 2017. Mitigating supply uncertainty: The interplay between diversification and pricing. *Prod. Oper. Manag.* 26 (3), 369–388. <http://dx.doi.org/10.1111/poms.12656>.
- Liu, A., Wang, X., Tang, J., 2024. Optimizing multi-channel procurement planning under disruption risks. *Int. J. Prod. Econ.* 275, 109346. <http://dx.doi.org/10.1016/j.ijpe.2024.109346>.
- Lotfi, R., Hazrati, R., Aghakhani, S., Afshar, M., Amra, M., Ali, S.S., 2024a. A data-driven robust optimization in viable supply chain network design by considering Open Innovation and Blockchain Technology. *J. Clean. Prod.* 436, 140369. <http://dx.doi.org/10.1016/j.jclepro.2023.140369>.
- Lotfi, R., Hazrati, H., Ali, S.S., Sharifmousavi, S.M., Khanbaba, A., Amra, M., 2023b. Antifragile, sustainable and agile healthcare waste chain network design by considering blockchain, resiliency, robustness and risk. *Cent. Eur. J. Oper. Res.* 1–34. <http://dx.doi.org/10.1007/s10100-023-00874-0>.
- Lotfi, R., Khanbaba, A., Ali, S.S., Afshar, M., Mehrjardi, M.S., Omidi, S., 2024b. Net-zero, resilience, and agile closed-loop supply chain network design considering robustness and renewable energy. *Env. Sci. Pollut. Res.* <http://dx.doi.org/10.1007/s11356-024-32661-y>.
- Lotfi, R., Mehrjardi, M.S., Ansari, P.M., Zolfaqari, F., Afshar, M., 2023a. Antifragile, sustainable, and agile supply chain network design by considering resiliency, robustness, risk, and environmental requirements. *Env. Sci. Pollut. Res.* 30 (48), 106442–106459. <http://dx.doi.org/10.1007/s11356-023-29488-4>.
- Lotfi, R., MohajerAnsari, P., Nevisi, M.M.S., Afshar, M., Davoodi, S.M.R., Ali, S.S., 2023d. A viable supply chain by considering vendor-managed-inventory with a consignment stock policy and learning approach. *Results Eng.* 21, 101609. <http://dx.doi.org/10.1016/j.rineng.2023.101609>.
- Lotfi, R., Nazarpour, H., Gharehbaghi, A., Sarkhosh, S.M.H., Khanbaba, A., 2022a. Viable closed-loop supply chain network by considering robustness and risk as a circular economy. *Env. Sci. Pollut. Res.* 29 (46), 70285–70304. <http://dx.doi.org/10.1007/s11356-022-20713-0>.
- Lotfi, R., Rajabzadeh, M., Zamani, A., Rajabi, M.S., 2022b. Viable supply chain with vendor-managed inventory approach by considering blockchain. *Risk Robust. Ann. Oper. Res.* 344 (2), 575–594. <http://dx.doi.org/10.1007/s10479-022-05119-y>.
- Lotfi, R., Shafei, R.M., Komeleh, M.G., Pasha, F.G., Ferasat, M., 2023c. Vaccine supply chain network design by considering viability, robustness and risk. *J. Eng. Res.* 13 (1), 27–38. <http://dx.doi.org/10.1016/j.jer.2023.10.007>.
- Modgil, S., Gupta, S., Stekelorum, R., Laguir, I., 2022. AI technologies and their impact on supply chain resilience during COVID-19. *Int. J. Phys. Distrib. Logist. Manag.* 52 (2), 130–149. <http://dx.doi.org/10.1108/IJPDLM-12-2020-0434>.
- Mohammadivojdan, R., Merzifonluoglu, Y., Geunes, J., 2022. Procurement portfolio planning for a newsvendor with supplier delivery uncertainty. *European J. Oper. Res.* 297 (3), 917–929. <http://dx.doi.org/10.1016/j.ejor.2021.05.026>.
- Mohammed, A., Bai, C., Channouf, N., Ahmed, T.A., Mohamed, S.M., 2023. G-resilient multi-tier supplier selection and order allocation in food industry: a hybrid methodology. *Int. J. Syst. Sci.: Oper. Logist.* 10 (1), 2195055. <http://dx.doi.org/10.1080/23302674.2023.2195055>.
- Namdar, J., Li, X., Sawhney, R., Pradhan, N., 2018. Supply chain resilience for single and multiple sourcing in the presence of disruption risks. *Int. J. Prod. Res.* 56 (6), 2339–2360. <http://dx.doi.org/10.1080/00207543.2017.1370149>.
- Niu, B., Li, J., Zhang, J., Cheng, H.K., Tan, Y., 2019. Strategic analysis of dual sourcing and dual channel with an unreliable alternative supplier. *Prod. Oper. Manag.* 28 (3), 570–587. <http://dx.doi.org/10.1111/poms.12938>.

- Pettit, T.J., Croxton, K.L., Fiksel, J., 2019. The evolution of resilience in supply chain management: a retrospective on ensuring supply chain resilience. *J. Bus. Logist.* 40 (1), 56–65. <http://dx.doi.org/10.1111/jbl.12202>.
- Rockafellar, R.T., Uryasev, S., 2002. Conditional value-at-risk for general loss distributions. *J. Bank. Finance.* 26 (7), 1443–1471. <http://dx.doi.org/10.2139/ssrn.267256>.
- Sarraf, S., Kushwaha, A.K., Kar, A.K., Dwivedi, Y.K., Giannakis, M., 2024. How did online misinformation impact stockouts in the e-commerce supply chain during COVID-19—A mixed methods study. *Int. J. Prod. Econ.* 267, 109064. <http://dx.doi.org/10.1016/j.ijpe.2023.109064>.
- Sawik, T., Sawik, B., 2024. Risk-averse decision-making to maintain supply chain viability under propagated disruptions. *Int. J. Prod. Res.* 62 (8), 2853–2867. <http://dx.doi.org/10.1080/00207543.2023.2236726>.
- Schultz, R., Tiedemann, S., 2003. Risk aversion via excess probabilities in stochastic programs with mixed-integer recourse. *SIAM J. Optim.* 14 (1), 115–138. <http://dx.doi.org/10.1137/S1052623402410855>.
- Shang, C., Huang, X., You, F., 2017. Data-driven robust optimization based on kernel learning. *Comput. Chem. Eng.* 106, 464–479. <http://dx.doi.org/10.1016/j.compchemeng.2017.07.004>.
- Suryadi, A., Rau, H., 2023. Considering region risks and mitigation strategies in the supplier selection process for improving supply chain resilience. *Comput. Ind. Eng.* 181, 109288. <http://dx.doi.org/10.1016/j.cie.2023.109288>.
- Svoboda, J., Minner, S., Yao, M., 2021. Typology and literature review on multiple supplier inventory control models. *European J. Oper. Res.* 293 (1), 1–23. <http://dx.doi.org/10.2139/ssrn.2995134>.
- Tang, S.Y., Gurnani, H., Gupta, D., 2014. Managing disruptions in decentralized supply chains with endogenous supply process reliability. *Prod. Oper. Manag.* 23 (7), 1198–1211. <http://dx.doi.org/10.1111/poms.12160>.
- Tang, S.Y., Kouvelis, P., 2011. Supplier diversification strategies in the presence of yield uncertainty and buyer competition. *Manuf. Serv. Oper. Manag.* 13 (4), 439–451. <http://dx.doi.org/10.1287/msom.1110.0337>.
- Wang, Y., Liu, Y., Bai, X., 2024a. Designing a new robust resilience supply chain network under partial distribution information. *Comput. Ind. Eng.* 190, 110028. <http://dx.doi.org/10.1016/j.cie.2024.110028>.
- Wang, Y., Liu, Y., Pei, H., 2024b. Designing a new robust solid waste recycling network under uncertainty: A case study about circular economy transition. *Soc.-Econ. Plan. Sci.* 96, 102066. <http://dx.doi.org/10.1016/j.seps.2024.102066>.
- Wu, F., Shu, L., Zhao, S.S., Jiang, B., 2020. Risk-averse portfolio procurement strategy under large-scale promotion online. *IEEE Trans. Eng. Manage.* 69 (4), 1252–1261. <http://dx.doi.org/10.1109/TEM.2020.2975237>.
- Wu, M., Zhang, J., Chen, X., 2025. Managing supply disruptions for risk-averse buyers: Diversified sourcing vs. Disrupt. *Prev. Omega* 131, 103217. <http://dx.doi.org/10.1016/j.omega.2024.103217>.
- Yin, Z., Wang, C., 2018. Strategic cooperation with a backup supplier for the mitigation of supply disruptions. *Int. J. Prod. Res.* 56 (12), 4300–4312. <http://dx.doi.org/10.1080/00207543.2017.1410246>.
- Yoon, J., Talluri, S., Rosales, C., 2020. Procurement decisions and information sharing under multi-tier disruption risk in a supply chain. *Int. J. Prod. Res.* 58 (5), 1362–1383. <http://dx.doi.org/10.1080/00207543.2019.1634296>.
- Zackrisson, A., Engholm, A., Tang, O., 2025. Data-driven analysis of strategic-operational interfaces in freight electrification under deep uncertainty. *Transp. Res. D: Transp. Env.* 139, 104524. <http://dx.doi.org/10.1016/j.trd.2024.104524>.
- Zhang, Y., Wang, Y., Bai, X., Liu, Y., 2024. Designing a robust sustainable service network for agricultural machinery maintenance under demand uncertainty. *Int. Trans. Oper. Res.* <http://dx.doi.org/10.1111/itor.13579>.